Published for SISSA by Springer

Received: May 6, 2020
Revised: June 19, 2020
Accepted: June 24, 2020
Published: August 4, 2020

Bayesian fit analysis to full distribution data of $\bar{B} \to D^{(*)}\ell\bar{\nu}$: $|V_{cb}|$ determination and new physics constraints

Syuhei Iguro[a] **and Ryoutaro Watanabe**[b]

[a] *Department of Physics, Nagoya University, Furo-cho Chikusa-ku, Nagoya 464-8602, Japan*
[b] *INFN, Sezione di Roma Tre, Via della Vasca Navale 84, Rome 00146, Italy*

E-mail: iguro@eken.phys.nagoya-u.ac.jp, ryoutaro.watanabe@roma3.infn.it

Abstract: We investigate the semi-leptonic decays of $\bar{B} \to D^{(*)}\ell\bar{\nu}$ in terms of the Heavy-Quark-Effective-Theory (HQET) parameterization for the form factors, which is described with the heavy quark expansion up to $\mathcal{O}(1/m_c^2)$ beyond the simple approximation considered in the original CLN parameterization. An analysis with this setup was first given in the literature, and then we extend it to the comprehensive analyses including (i) simultaneous fit of $|V_{cb}|$ and the HQET parameters to available experimental full distribution data and theory constraints, and (ii) New Physics (NP) contributions of the V_2 and T types, such as $(\bar{c}\gamma^\mu P_R b)(\bar{\ell}\gamma_\mu P_L \nu_\ell)$ and $(\bar{c}\sigma^{\mu\nu} P_L b)(\bar{\ell}\sigma_{\mu\nu} P_L \nu_\ell)$, to the decay distributions and rates. For this purpose, we perform Bayesian fit analyses by using `Stan` program, a state-of-the-art public platform for statistical computation. Then, we show that our $|V_{cb}|$ fit results for the SM scenarios are close to the PDG combined average from the exclusive mode, and indicate significance of the angular distribution data. In turn, for the SM + NP scenarios, our fit analyses find that non-zero NP contribution is favored at the best fit point for both SM + V_2 and SM + T depending on the HQET parameterization model. A key feature is then realized in the $\bar{B} \to D^{(*)}\tau\bar{\nu}$ observables. Our fit result of the HQET parameters in the SM(+T) produces a consistent value for R_D while smaller for R_{D^*}, compared with the previous SM prediction in the HFLAV report. On the other hand, SM + V_2 points to smaller and larger values for R_D and R_{D^*} than the SM predictions. In particular, the R_{D^*} deviation from the experimental measurement becomes smaller, which could be interesting for future improvement on measurements at the Belle II experiment.

Keywords: Phenomenological Models

ArXiv ePrint: 2004.10208

https://doi.org/10.1007/JHEP08(2020)006

JHEP08(2020)006

Contents

JHEP08(2020)006

1 Introduction

The semi-leptonic processes $\bar{B} \to D^{(*)}\ell\bar{\nu}$ for $\ell = e, \mu$ have been studied from various perspectives. In particular, the decay rates are of great interest as it determines the Cabibbo-Kobayashi-Maskawa [1, 2] (CKM) matrix element $|V_{cb}|$ in the Standard Model (SM). Kinetic distributions of the processes are also important, for instance, to experimentally measure the ratios with the semi-tauonic modes, $R_{D^{(*)}} = \mathcal{B}(\bar{B} \to D^{(*)}\tau\bar{\nu})/\mathcal{B}(\bar{B} \to D^{(*)}\ell\bar{\nu})$, in which discrepancies between the experimental measurements and the SM predictions have been reported [3].

To investigate these issues, however, we need a sufficient knowledge on the hadron transitions $\bar{B} \to D^{(*)}$. In the literature, there are several theoretical descriptions on the form factors (FFs). The CLN parameterization [4], applying heavy quark symmetry to FFs

based on the Heavy-Quark-Effective-Theory [5, 6] (HQET), has been used for this purpose. The BGL parameterization [7] is an alternative that relies only on QCD dispersion relations, which implies the model independent one.

An advantage of the former is that it describes the $\bar{B} \to D$ and $\bar{B} \to D^*$ FFs with a few common parameters, and thus a combined analysis is possible, e.g., see ref. [8]. The latter, on the other hand, includes larger number of independent parameters so that a flexible fit analysis is given, although it needs experimental data with higher statistics. Then, the $|V_{cb}|$ determinations from these two approaches have been in the spotlight since their results are not consistent with each other, see discussions in refs. [9–15].

In the recent studies of refs. [16, 17], the authors have revisited the HQET parameterization by adopting a setup beyond the CLN approximation and taking $1/m_c^2$ corrections into account for the heavy quark expansion. Then the authors have proposed two viable parameterization models introducing 13 and 23 free HQET parameters, respectively, which have to be determined from experiments and/or theoretical constraints (as also explained in this paper). At the expense of such a large number of parameter set, it has been found [17] that the SM fit result of $|V_{cb}|$ is in good agreement with the one obtained from the BGL parameterization. This conclusion, however, implies that $|V_{cb}|$ from the exclusive mode is still not fully consistent with the one from the inclusive mode, referred to as V_{cb} puzzle [18].

In this paper, we investigate $\bar{B} \to D^{(*)}\ell\bar{\nu}$ with the use of this HQET parameterization by concerning the following points:

- We include all the available full distribution data of $\bar{B} \to D^{(*)}\ell\bar{\nu}$ from the Belle measurements [19–21] in our fit analysis[1] to *simultaneously* determine $|V_{cb}|$ and the HQET parameters. Indeed, this is not the case for the reference as will be explained later.

- We consider New Physics (NP) effects on $\bar{B} \to D^{(*)}\ell\bar{\nu}$ that could affect both branching ratios and decay distributions. Here, a simultaneous fit for the size of the NP contributions, $|V_{cb}|$, and the HQET parameters is performed in our analysis to see whether the V_{cb} puzzle can be resolved and/or a further fit improvement is possible. Then it is shown that a non-negligible NP contribution is still allowed and it satisfies the experimental data. We also provide complete formulae on the decay distributions and the FFs in the presence of NP.

- We perform Bayesian fit analysis with the use of `Stan` [23, 24], a public platform for statistical computation, which has been widely known in the statistical science community and thus could give independent check to the previous studies. We also obtain quantitative evaluations on our fit results in various parameterization scenarios with/without NP by looking at *information criterion* [25].

In addition, we put a comparison between the CLN and HQET parameterizations to see where its difference comes out. Then, finally we show our predictions on the $\bar{B} \to D^{(*)}\tau\bar{\nu}$

[1] The BaBar experimental analysis is given in ref. [22], but they do not provide detailed information on distribution data.

JHEP08(2020)006

observables. As a result, we will see that *NP predictions* on $R_{D^{(*)}}$ obtained from our fit results are different from the SM predictions, and that this could be a key feature for the NP search in the $\bar{B} \to D^{(*)}\tau\bar{\nu}$ observables. We would like to stress that this is a comprehensive fit analysis for the HQET parameterization with/without the NP contributions.

This paper is organized as follows. In section 2, we describe our theory setup for the HQET parameterization and formulae for the decay distributions in the presence of NP. In section 3, we detail our fit procedure along with summary of theory constraints and experimental measurements to be taken in our analysis. Then we discuss our results in the various scenarios. Finally, a summary is put in section 4. Details of our fit results, distribution formulae, and some theory constraints are given in appendices.

2 Theory setup

In this work, we start with the effective Hamiltonian that affects $\bar{B} \to D^{(*)}\ell\bar{\nu}$, given as

$$\mathcal{H}_{\rm eff} = \frac{4G_F}{\sqrt{2}} V_{cb} \Big[(\bar{c}\gamma^\mu P_L b)(\bar{\ell}\gamma_\mu P_L \nu_\ell) + C_{V_2}(\bar{c}\gamma^\mu P_R b)(\bar{\ell}\gamma_\mu P_L \nu_\ell) + C_T(\bar{c}\sigma^{\mu\nu} P_L b)(\bar{\ell}\sigma_{\mu\nu} P_L \nu_\ell) \Big], \tag{2.1}$$

where $P_{L/R} = (1 \mp \gamma_5)/2$ and $C_{T(V_2)} \neq 0$ indicates existence of a tensor ($V + A$ vector in $\bar{c}b$) type NP. The SM-like NP always rescales V_{cb} and then we do not consider this case since its effect has to be examined by indirect or combined approaches. As long as the light lepton mode ($\ell = e, \mu$) is concerned, note that the scalar type operators, $(\bar{c}P_R b)(\bar{\ell}P_L\nu_\ell)$ and $(\bar{c}P_L b)(\bar{\ell}P_L\nu_\ell)$, do not affect the present processes due to the light lepton mass suppression. We assume that NP has e–μ universal ($C_X^e = C_X^\mu \equiv C_X$) and C_X is real. This is a conservative choice since $\mathcal{B}(\bar{B} \to D^{(*)}\mu\bar{\nu})/\mathcal{B}(\bar{B} \to D^{(*)}e\bar{\nu}) \approx 1 \pm \mathcal{O}(\%)$ has been reported [19–21]. Also the neutrino is always taken as left-handed.

In the following part of this section, we will present theory descriptions and formulae necessary for our fit analysis.

2.1 HQET description of form factors

In the HQET basis, all possible types of the $B \to D^{(*)}$ current are defined as

$$\langle D|\bar{c}\gamma^\mu b|B\rangle_{\rm HQET} = \sqrt{m_B m_D}\big[h_+(v+v')^\mu + h_-(v-v')^\mu\big]\,, \tag{2.2}$$

$$\langle D|\bar{c}b|B\rangle_{\rm HQET} = \sqrt{m_B m_D}(w+1)h_S\,, \tag{2.3}$$

$$\langle D|\bar{c}\sigma^{\mu\nu}b|B\rangle_{\rm HQET} = -i\sqrt{m_B m_D}\,h_T\big[v^\mu v'^\nu - v'^\mu v^\nu\big]\,, \tag{2.4}$$

$$\langle D^*|\bar{c}\gamma^\mu b|B\rangle_{\rm HQET} = i\sqrt{m_B m_{D^*}}h_V\varepsilon^{\mu\nu\rho\sigma}\epsilon^*_\nu v'_\rho v_\sigma\,, \tag{2.5}$$

$$\langle D^*|\bar{c}\gamma^\mu\gamma^5 b|B\rangle_{\rm HQET} = \sqrt{m_B m_{D^*}}\big[h_{A_1}(w+1)\epsilon^{*\mu} - (\epsilon^*\cdot v)\left(h_{A_2}v^\mu + h_{A_3}v'^\mu\right)\big]\,, \tag{2.6}$$

$$\langle D^*|\bar{c}\gamma^5 b|B\rangle_{\rm HQET} = -\sqrt{m_B m_{D^*}}(\epsilon^*\cdot v)h_P\,, \tag{2.7}$$

$$\begin{aligned}\langle D^*|\bar{c}\sigma^{\mu\nu}b|B\rangle_{\rm HQET} = -\sqrt{m_B m_{D^*}}\varepsilon^{\mu\nu\rho\sigma}\big[&h_{T_1}\epsilon^*_\rho(v+v')_\sigma + h_{T_2}\epsilon^*_\rho(v-v')^\sigma \\ &+ h_{T_3}(\epsilon^*\cdot v)(v+v')_\rho(v-v')_\sigma\big]\,,\end{aligned} \tag{2.8}$$

where $v^\mu = p_B^\mu/m_B$, $v'^\mu = p^\mu_{D^{(*)}}/m_{D^{(*)}}$, $w = v\cdot v' = (m_B^2 + m^2_{D^{(*)}} - q^2)/(2m_B m_{D^{(*)}})$, and $h_X \equiv h_X(w)$ are the HQET form factors in terms of w. Then, h_X can be represented by the

JHEP08(2020)006

leading Isgur-Wise [5] (IW) function ξ and its correction, defined as $h_X(w) = \xi(w)\hat{h}_X(w)$. In this work, we consider

$$\hat{h}_X = \hat{h}_{X,0} + \frac{\alpha_s}{\pi}\delta\hat{h}_{X,\alpha_s} + \frac{\bar{\Lambda}}{2m_b}\delta\hat{h}_{X,m_b} + \frac{\bar{\Lambda}}{2m_c}\delta\hat{h}_{X,m_c} + \left(\frac{\bar{\Lambda}}{2m_c}\right)^2 \delta\hat{h}_{X,m_c^2}\,, \tag{2.9}$$

where

$$\hat{h}_{X,0} = \begin{cases} 1 & \text{for } X = +, A_1, A_3, S, P, T, T_1 \\ 0 & \text{for } X = -, A_2, T_2, T_3 \end{cases}, \tag{2.10}$$

and others indicate higher order corrections in α_s and $1/m_{b,c}$ expansions. In this work, the above HQET expansion is given at the matching scale $\mu_b = 4.2\,\text{GeV}$ with values for the expansion coefficients to be fixed as $\epsilon_a = \alpha_s/\pi = 0.0716$, $\epsilon_b = \bar{\Lambda}/(2m_b) = 0.0522$, and $\epsilon_c = \bar{\Lambda}/(2m_c) = 0.1807$. Possible uncertainties to the coefficients from quark masses are rather small, and also essentially correspond to rescaling of $\delta\hat{h}_{X,f}$. Thus we neglect those uncertainties hereafter. The complete expressions for $\delta\hat{h}_{X,f}$ are summarized in appendix A.

The $1/m_Q$ correction consists of three unknown sub-leading IW functions defined as $\xi_3(w)$, $\chi_2(w)$, and $\chi_3(w)$ [8], whereas $1/m_Q^2$ of six subsub-leading IW functions $\ell_{1\text{–}6}(w)$ [26]. Thus we have in total ten IW functions that are in principle unknown and then have to be fitted. We also employ the notation such as

$$\eta(w) = \frac{\xi_3(w)}{\xi(w)}\,, \quad \hat{\chi}_i(w) = \frac{\chi_i(w)}{\xi(w)}\,, \quad \hat{\ell}_i(w) = \frac{\ell_i(w)}{\xi(w)}\,. \tag{2.11}$$

Then, we can express any of the IW functions by means of series expansion around $w = 1$. Namely, we take

$$f(w) = \sum_{n=0} \frac{f^{(n)}}{n!}(w-1)^n\,, \tag{2.12}$$

for $f = \xi$, η, $\hat{\chi}_i$, and $\hat{\ell}_i$. Here, $f^{(n)} \equiv \frac{\partial^n f(w)}{\partial w^n}\Big|_{w=1}$ are free parameters to be fitted by theoretical and/or experimental analysis. Analytic properties of the matrix elements indicate that the above expansion can be represented by

$$w(z) = 2\left(\frac{1+z}{1-z}\right)^2 - 1\,, \tag{2.13}$$

up to the order of interest. For instance, we have

$$f(w) = f^{(0)} + 8f^{(1)}z + 16\left(f^{(1)} + 2f^{(2)}\right)z^2 + \frac{8}{3}\left(9f^{(1)} + 48f^{(2)} + 32f^{(3)}\right)z^3 + \mathcal{O}(z^4)\,. \tag{2.14}$$

Note that $\xi^{(0)} = 1$ and $\hat{\chi}_3^{(0)} = 0$ in the HQET description. Following ref. [17], the cases of

$$\text{NNLO}(3/2/1)\ :\ \xi(w) \text{ up to } z^3\,,\ \ \hat{\chi}_{2,3}(w) \text{ and } \eta(w) \text{ up to } z^2\,,\ \ \hat{\ell}_{1\text{–}6}(w) \text{ up to } z^1\,, \tag{2.15}$$

$$\text{NNLO}(2/1/0)\ :\ \xi(w) \text{ up to } z^2\,,\ \ \hat{\chi}_{2,3}(w) \text{ and } \eta(w) \text{ up to } z^1\,,\ \ \hat{\ell}_{1\text{–}6}(w) \text{ up to } z^0\,, \tag{2.16}$$

JHEP08(2020)006

are investigated in our analysis. In addition, we consider

$$\text{NLO}(3/2/-)\ :\ \xi(w)\text{ up to }z^3\,,\ \ \hat{\chi}_{2,3}(w)\text{ and }\eta(w)\text{ up to }z^2\,,\ \ \hat{\ell}_{1\text{–}6}(w)=0\,, \tag{2.17}$$

just for comparison to see how $\hat{\ell}_{1\text{–}6}(w)$ improves the parameter fit. Throughout this paper, we refer them to as the HQET parameterizations.

A final remark is that we have two kinds of expansion, namely, by $\epsilon_{a,b,c}$ and z in the form factor $\hat{h}_X$. A significant point is that their highest orders, as assumed above, have to be kept in observables even though it is obtained by multiplying $\hat{h}_X$s. Otherwise, higher order terms than what we take are included unfairly. Schematically, a proper expansion for any observable is written as

$$\begin{aligned}\text{Obs.} =\ &\mathcal{O}(\epsilon^0 z^0)+\mathcal{O}(\epsilon^0 z^1)+\mathcal{O}(\epsilon^0 z^2)+\mathcal{O}(\epsilon^0 z^3)+\mathcal{O}(\epsilon_a^1 z^0)+\mathcal{O}(\epsilon_a^1 z^1)+\mathcal{O}(\epsilon_a^1 z^2)+\mathcal{O}(\epsilon_a^1 z^3)\\ &+\mathcal{O}(\epsilon_{b,c}^1 z^0)+\mathcal{O}(\epsilon_{b,c}^1 z^1)+\mathcal{O}(\epsilon_{b,c}^1 z^2)+\mathcal{O}(\epsilon_c^2 z^0)+\mathcal{O}(\epsilon_c^2 z^1)\,,\end{aligned} \tag{2.18}$$

before the w integration, where $\epsilon_a=\alpha_s/\pi$ and $\epsilon_{b,c}=\bar{\Lambda}/(2m_{b,c})$.

2.2 Formula for $\bar{B}\to D\ell\bar{\nu}$: w distribution

The differential decay rate of $\bar{B}\to D\ell\bar{\nu}$ with respect to w is written as

$$\frac{d\Gamma_D}{dw}=G_F^2|V_{cb}|^2\frac{m_B m_D^2\eta_{\text{EW}}^2}{48\pi^3}(1-2r_D w+r_D^2)\sqrt{w^2-1}\Big[(1+C_{V_2})^2H_s(w)^2+2|C_T|^2H_s^T(w)^2\Big]\,, \tag{2.19}$$

where $r_D=m_D/m_B$ and $\eta_{\text{EW}}=1.0066\pm0.0050$ accounts for the leading electroweak corrections [27, 28]. The Hadronic Amplitudes are given as [29–31]

$$\begin{aligned}H_s(w)&=m_B\sqrt{r_D}\frac{\sqrt{w^2-1}}{\sqrt{1-2r_D w+r_D^2}}\left[(1+r_D)h_+(w)-(1-r_D)h_-(w)\right]\,,\\ H_s^T(w)&=-m_B\sqrt{r_D}\sqrt{w^2-1}\,h_T(w)\,.\end{aligned} \tag{2.20}$$

Note that the tensor NP do not interfere with the SM since the ℓ helicity is flipped in the massless limit of the light lepton due to spin structure of $\bar{\ell}\sigma^{\mu\nu}\nu$. One can see that

$$\mathcal{G}(w)=h_+(w)-\frac{1-r_D}{1+r_D}h_-(w)\,, \tag{2.21}$$

is the usual normalization factor for the SM. The FFs $h_X(w)$ are then represented with the HQET parameterizations for our analysis.

In the CLN parameterization, it is approximated with a single parameter such as $\mathcal{G}(w)\approx\mathcal{G}(1)\left[1-8\rho^2 z+(51\rho^2-10)z^2-(252\rho^2-84)z^3\right]$. Comparing it with the present forms of $h_\pm(w)$ for the case of NNLO(3/2/1), we obtain

$$\mathcal{G}(1)\simeq 1.0883-0.1227\eta^{(0)}+0.0327\hat{\ell}_1^{(0)}-0.0156\hat{\ell}_4^{(0)}\,, \tag{2.22}$$

$$\begin{aligned}-8\rho^2\mathcal{G}(1)\simeq\ &0.3751+8.7061\xi^{(1)}-7.4528\hat{\chi}_2^{(0)}+22.3584\hat{\chi}_3^{(1)}-0.9816\big(\eta^{(1)}+\eta^{(0)}\xi^{(1)}\big)\\ &+0.2612\big(\hat{\ell}_1^{(1)}+\hat{\ell}_1^{(0)}\xi^{(1)}\big)-0.1247\big(\hat{\ell}_4^{(1)}+\hat{\ell}_4^{(0)}\xi^{(1)}\big)\,,\end{aligned} \tag{2.23}$$

JHEP08(2020)006

in our setup. We can see that the NNLO parameters $\hat{\ell}^{(n)}_{1,4}$ affect these quantities. As for the z^2 and z^3 terms, the HQET parameterizations take lengthy forms while the CLN gives the above approximate expressions by the single parameter ρ^2. We will show the latter approximation underestimates uncertainties in these terms.

2.3 Formula for $\bar{B} \to D^* \ell \bar{\nu}$: full angular distribution

Concerning the available experimental data, we show the full differential decay rate for $B^0 \to D^{*-}(\to \bar{D}^0 \pi^-)\ell\bar{\nu}$ in the presence of the NP contributions:

$$\frac{d\Gamma^{\rm full}_{D^*}}{dw\, d\cos\theta_\ell\, d\cos\theta_V\, d\chi} = \mathcal{B}(D^{*-} \to \bar{D}^0\pi^-) G_F^2 |V_{cb}|^2 \frac{3 m_B m_{D^*}^2 \eta_{\rm EW}^2}{4(4\pi)^4} \times (1 - 2 r_{D^*} w + r_{D^*}^2)\sqrt{w^2-1} \sum_{i=1}^{6} \mathcal{J}_i(\theta_\ell, \theta_V, \chi) \mathcal{H}_i(w)\,, \tag{2.24}$$

where $\mathcal{J}_i$ include angular dependences[2] obtained as

$$\begin{aligned}
&\mathcal{J}_1 = (1-\cos\theta_\ell)^2 \sin^2\theta_V\,, && \mathcal{J}_2 = (1+\cos\theta_\ell)^2 \sin^2\theta_V\,,\\
&\mathcal{J}_3 = 4\sin^2\theta_\ell \cos^2\theta_V && \mathcal{J}_4 = -2\sin^2\theta_\ell \sin^2\theta_V \cos 2\chi\,,\\
&\mathcal{J}_5 = -4\sin\theta_\ell (1-\cos\theta_\ell)\sin\theta_V\cos\theta_V\cos\chi\,,\\
&\mathcal{J}_6 = +4\sin\theta_\ell (1+\cos\theta_\ell)\sin\theta_V\cos\theta_V\cos\chi\,,\\
&\mathcal{J}_7 = 2\sin^2\theta_\ell \sin^2\theta_V\,, && \mathcal{J}_8 = 8\cos^2\theta_\ell \cos^2\theta_V\,,
\end{aligned} \tag{2.25}$$

and $\mathcal{H}_i$ indicate hadronic parts described as

$$\begin{aligned}
\mathcal{H}_1(w) &= \Big(H_+(w) - C_{V_2} H_-(w)\Big)^2\,,\\
\mathcal{H}_2(w) &= \Big(H_-(w) - C_{V_2} H_+(w)\Big)^2\,,\\
\mathcal{H}_3(w) &= (1-C_{V_2})^2 H_0(w)^2\,,\\
\mathcal{H}_4(w) &= \Big(H_+(w) - C_{V_2} H_-(w)\Big)\Big(H_-(w) - C_{V_2} H_+(w)\Big) + 16|C_T|^2 H_-^T(w) H_+^T(w)\,,\\
\mathcal{H}_5(w) &= (1-C_{V_2}) H_0(w)\Big(H_+(w) - C_{V_2} H_-(w)\Big) + 8|C_T|^2\Big(H_0^T(w) H_-^T(w) - H_0^T(w) H_+^T(w)\Big)\,,\\
\mathcal{H}_6(w) &= (1-C_{V_2}) H_0(w)\Big(H_-(w) - C_{V_2} H_+(w)\Big) + 8|C_T|^2\Big(H_0^T(w) H_-^T(w) - H_0^T(w) H_+^T(w)\Big)\,,\\
\mathcal{H}_7(w) &= 8|C_T|^2\Big(H_+^T(w)^2 + H_-^T(w)^2\Big)\,,\\
\mathcal{H}_8(w) &= 8|C_T|^2 H_0^T(w)^2\,.
\end{aligned} \tag{2.26}$$

Note again that there is no interference term between the vector and tensor currents. Then, we can write the Hadronic Amplitudes $H_n^{(T)}$ from refs. [29–31] as

$$\begin{aligned}
H_\pm(w) &= m_B \sqrt{r_{D^*}} \left[(w+1) h_{A_1}(w) \mp \sqrt{w^2-1}\, h_V(w)\right]\,,\\
H_0(w) &= m_B \sqrt{r_{D^*}} \frac{\sqrt{w^2-1}}{\sqrt{1-2r_{D^*}w+r_{D^*}^2}} \left[(r_{D^*}-w) h_{A_1}(w) + (w-1)(r_{D^*} h_{A_2}(w) + h_{A_3}(w))\right]\,,
\end{aligned}$$

[2] Note that the definition of θ_ℓ here is not the same as θ_τ in ref. [29], but related as $\theta_\ell = \pi - \theta_\tau$.

JHEP08(2020)006

$$H_{\pm}^{T}(w) = m_B\sqrt{r_{D^*}}\frac{1-r_{D^*}(w\mp\sqrt{w^2-1})}{\sqrt{1-2r_{D^*}w+r_{D^*}^2}} \times\Big[h_{T_1}(w)+h_{T_2}(w)+(w\pm\sqrt{w^2-1})(h_{T_1}(w)-h_{T_2}(w))\Big]\,,$$
$$H_{0}^{T}(w) = -m_B\sqrt{r_{D^*}}\Big[(w+1)h_{T_1}(w)+(w-1)h_{T_2}(w)+2(w^2-1)h_{T_3}(w)\Big]\,. \tag{2.27}$$

The angular dependence of eq. (2.25) can be derived as explained in appendix B. The normalization factor is given as $\mathcal{F}(1) = h_{A_1}(1)$ and then the HQET parameterization leads to

$$\mathcal{F}(1) \simeq 0.9702 + 0.0327\hat{\ell}_2^{(0)}\,, \tag{2.28}$$

and its w dependence takes a lengthy form, (and hence omitted).

In the CLN parameterization, on the other hand, the w dependence on $\mathcal{F}(w)$ is approximated by using the following functions: $h_{A_1}(w)$ with the slope $\rho^2_{D^*}$ similar to $\mathcal{G}(w)$, $R_1(w) \equiv h_V(w)/h_{A_1}(w)$, and $R_2(w) \equiv \big(h_{A_3}(w) + r_{D^*}h_{A_2}(w)\big)/h_{A_1}(w)$, where the latter two are expanded in $(w-1)$. But, this simplification is not proper for the present parameterization since it conflicts with the $\epsilon_{a,b,c}$ and z expansions which we explained as in eq. (2.18). Instead, we will provide a more straightforward fit result by means of the z expansion for $\mathcal{F}(w)$.

3 Fit analysis

3.1 Theory constraints on form factors

There are theoretical studies to evaluate the form factors at specific points of w with respect to the following quantities:

$$f_+^{B\to D}(w) = \frac{1}{2\sqrt{r_D}}\Big[\,(1+r_D)\,h_+(w) - (1-r_D)\,h_-(w)\Big]\,, \tag{3.1}$$
$$f_0^{B\to D}(w) = \sqrt{r_D}\left[\frac{w+1}{1+r_D}h_+(w) + \frac{w-1}{1-r_D}h_-(w)\right]\,, \tag{3.2}$$
$$f_T^{B\to D}(w) = \frac{1+r_D}{2\sqrt{r_D}}h_T(w)\,, \tag{3.3}$$
$$A_1^{B\to D^*}(w) = \frac{\sqrt{r_{D^*}}(1+w)}{1+r_{D^*}}h_{A_1}(w)\,, \tag{3.4}$$
$$A_0^{B\to D^*}(w) = \frac{1}{2\sqrt{r_{D^*}}}\Big[(w+1)h_{A_1}(w) + (w\,r_{D^*}-1)h_{A_2}(w) + (r_{D^*}-w)h_{A_3}(w)\Big]\,, \tag{3.5}$$
$$V^{B\to D^*}(w) = \frac{1+r_{D^*}}{2\sqrt{r_{D^*}}}h_V(w)\,, \tag{3.6}$$
$$T_1^{B\to D^*}(w) = \frac{1}{2\sqrt{r_{D^*}}}\Big[(1+r_{D^*})h_{T_1}(w) - (1-r_{D^*})h_{T_2}(w)\Big]\,, \tag{3.7}$$

JHEP08(2020)006

$$T_2^{B\to D^*}(w) = \sqrt{r_{D^*}}\left[\frac{w+1}{1+r_{D^*}}h_{T_1}(w) - \frac{w-1}{1-r_{D^*}}h_{T_2}(w)\right], \tag{3.8}$$

$$T_{23}^{B\to D^*}(w) = \frac{1+r_{D^*}}{4\sqrt{r_{D^*}}}\Big[(w+1)h_{T_1}(w) + (w-1)h_{T_2}(w) - (w^2-1)h_{T_3}(w)\Big]. \tag{3.9}$$

Then, the lattice studies [32–34] provide the following evaluations

$$f_+^{B\to D}(\{1,\ 1.08,\ 1.16\}) = \{1.1994(95),\ 1.0941(104),\ 1.0047(123)\}, \tag{3.10}$$

$$f_0^{B\to D}(\{1,\ 1.08,\ 1.16\}) = \{0.9026(72),\ 0.8609(77),\ 0.8254(94)\}, \tag{3.11}$$

$$h_{A_1}(1) = 0.904 \pm 0.012. \tag{3.12}$$

In ref. [35], the form factors at $q^2 = \{0, -5, -10, -15\}\text{GeV}^2$ have been evaluated by a light-cone sum rule (LCSR) approach. The result can be summarized as

$$f_+^{B\to D}(\{1.59,\ 1.84,\ 2.10,\ 2.35\}) = \{0.65(8),\ 0.55(7),\ 0.48(6),\ 0.42(5)\}, \tag{3.13}$$

$$f_0^{B\to D}(\{1.84,\ 2.10,\ 2.35\}) = \{0.62(8),\ 0.59(7),\ 0.56(7)\}, \tag{3.14}$$

$$f_T^{B\to D}(\{1.59,\ 1.84,\ 2.10,\ 2.35\}) = \{0.57(5),\ 0.46(3),\ 0.38(3),\ 0.33(2)\}, \tag{3.15}$$

$$A_1^{B\to D^*}(\{1.50,\ 1.74,\ 1.98,\ 2.21\}) = \{0.60(9),\ 0.56(9),\ 0.53(9),\ 0.50(8)\}, \tag{3.16}$$

$$A_0^{B\to D^*}(\{1.74,\ 1.98,\ 2.21\}) = \{0.55(8),\ 0.47(7),\ 0.40(7)\}, \tag{3.17}$$

$$V^{B\to D^*}(\{1.50,\ 1.74,\ 1.98,\ 2.21\}) = \{0.69(13),\ 0.59(11),\ 0.50(9),\ 0.44(8)\}, \tag{3.18}$$

$$T_1^{B\to D^*}(\{1.50,\ 1.74,\ 1.98,\ 2.21\}) = \{0.63(10),\ 0.54(9),\ 0.45(8),\ 0.39(7)\}, \tag{3.19}$$

$$T_2^{B\to D^*}(\{1.74,\ 1.98,\ 2.21\}) = \{0.60(10),\ 0.58(10),\ 0.55(10)\}, \tag{3.20}$$

$$T_{23}^{B\to D^*}(\{1.50,\ 1.74,\ 1.98,\ 2.21\}) = \{0.81(11),\ 0.74(11),\ 0.69(10),\ 0.65(10)\}, \tag{3.21}$$

where $w = \{1.59, \cdots\}$ and $w = \{1.50, \cdots\}$ correspond to $q^2 = \{0, \cdots\}$ for $B \to D$ and $B \to D^*$, respectively. Thanks to this comprehensive work, for instance, a fit analysis to "theory constraints only" is even possible.

In addition, QCD sum rule (QCDSR) can evaluate the sub-leading IW functions as in refs. [36–38]. By using formulae in the literature with updated QCD input data, we derive the following constraints

$$-0.08 < \hat{\chi}_2^{(0)} < -0.04, \qquad -0.02 < \hat{\chi}_2^{(1)} < +0.02, \qquad -0.03 < \hat{\chi}_2^{(2)} < +0.01, \tag{3.22}$$

$$+0.01 < \hat{\chi}_3^{(1)} < +0.06, \qquad -0.07 < \hat{\chi}_3^{(2)} < +0.02, \tag{3.23}$$

$$+0.50 < \eta^{(0)} < +0.73, \qquad +0.01 < \eta^{(1)} < +0.07, \qquad -0.12 < \eta^{(2)} < -0.02. \tag{3.24}$$

We show a detail of these constraints in appendix C.

In addition, we need to take care of Unitarity Bound (UB) for the case of the HQET parameterization. Following eqs. (5)–(20) of ref. [4], we obtain the functions U_{J^P} in terms of the present HQET parameters to be constrained by

$$U_{0^+} < \chi_{0^+}(0) \approx (5.96 \pm 0.44) \times 10^{-3}, \tag{3.25}$$

$$U_{0^-} < \tilde{\chi}_{0^-}(0) \approx (1.33 \pm 0.04) \times 10^{-2}, \tag{3.26}$$

$$U_{1^+} < m_{B^*} m_{D^*} \chi_{1^+}(0) \approx (3.90 \pm 0.16) \times 10^{-3}, \tag{3.27}$$

$$U_{1^-} < m_{B^*} m_{D^*} \tilde{\chi}_{1^-}(0) \approx (3.58 \pm 0.18) \times 10^{-3}, \tag{3.28}$$

JHEP08(2020)006

where the explicit forms of U_{J^P} are a bit lengthy and thus we attached a `Mathematica` file as supplementary material. The above numerical bounds are obtained by using recent data of (excited) B_c states [39, 40] and quark masses [18], instead of the original one [4].

For now, we leave discussion on how we take the uncertainties of these theoretical constraints in our fit analysis. It will be explained in section 3.3, and discussed in section 3.4.4.

3.2 Experimental data

The kinetic distributions of $\bar{B} \to D^{(*)}\ell\bar{\nu}$ have been measured by the Belle collaboration in refs. [19–21]. Available experimental data are then w distributions of $\bar{B} \to D\ell\bar{\nu}$ [19] (denoted as Belle15), and full kinetic $(w, \theta_\ell, \theta_V, \chi)$ distributions of $\bar{B} \to D^*\ell\bar{\nu}$ with the successive decay $D^* \to D\pi$ [20, 21]. The latter includes two independent measurements; one with hadronic tagging [20] (Belle17) and with untagged approach [21] for each e and μ mode (Belle18-e and Belle18-μ).

The Belle15 data correspond to the binned decay rate with respect to w, where the four processes, $\bar{B}^0 \to D^+ e^- \bar{\nu}$, $\bar{B}^0 \to D^+ \mu^- \bar{\nu}$, $\bar{B}^- \to D^0 e^- \bar{\nu}$, and $\bar{B}^- \to D^0 \mu^- \bar{\nu}$, are combined. The Belle17 data are given in terms of the unfolded decay rate of $\bar{B}^0 \to D^{*+}\ell^-\bar{\nu}$ for a corresponding bin $\frac{\Delta\Gamma}{\Delta x}$. This is derived from eq. (2.24) as

$$\frac{\Delta\Gamma}{\Delta x} = \frac{1}{\mathcal{B}(D^{*+} \to D^0\pi^+)} \int_{\Delta x} \frac{d\Gamma^{\rm full}_{D^*}}{dx}\,, \tag{3.29}$$

for $x = (w, \cos\theta_\ell, \cos\theta_V, \chi)$. On the other hand, the Belle18 data are shown in terms of binned signal event $\frac{\Delta N}{\Delta x}\big|_i$ (for i-th bin) in which the folded effect is presented by Response Matrix $\mathcal{R}$ together with efficiency ε among the bins. This is obtained as

$$\left.\frac{\Delta N}{\Delta x}\right|_i = N_{B^0}\,\tau_{B^0}\,\mathcal{B}(\bar{D}^0 \to K^-\pi^+)\,\mathcal{R}_{ij}\,\varepsilon_j \int_{\Delta x_j} \frac{d\Gamma^{\rm full}_{D^*}}{dx}\,, \tag{3.30}$$

where N_{B^0}, $\mathcal{R}_{ij}$, and ε_j are provided in ref. [21] for each e and μ modes.

Furthermore, we also take the world averages of the branching ratios (BR) of $\bar{B} \to D^{(*)}\ell\bar{\nu}$ [18] in our fit. A short summary for the experimental data and the theory constraints is shown in table 1. Correlations among the bins for each measurement are also taken into account in our fit analysis, (see corresponding references).

3.3 Fit procedure

In this work, a Bayesian fit analysis is applied to obtain allowed ranges of the HQET parameters and $|V_{cb}|$ with the use of Markov-Chain-Monte-Carlo (MCMC) method by `Stan` [23, 24], *a state-of-the-art platform for statistical modeling and high-performance statistical computation*, implemented in `MathematicaStan`.[3] The analysis is performed by MCMC runs involving 10 chains with Hamiltonian Monte Carlo algorithm giving 10^4 sampling points for every fit.

Although `Stan` is widely known in the statistical science community, it has not often been used in particle physics analysis. This enables us to give independent check of fit results obtained from public/private codes developed by particle physicists.

[3] For documentation and usage, see [41].

JHEP08(2020)006

Name	Object	Description
Belle15 [19]	$\bar{B} \to D\ell\bar{\nu}$	w distribution (10)
Belle17 [20]	$\bar{B}^0 \to D^{*+}\ell^-\bar{\nu}$	$(w, \theta_\ell, \theta_V, \chi)$ distributions (40)
Belle18-e [21]	$\bar{B}^0 \to D^{*+}e^-\bar{\nu}$	$(w, \theta_\ell, \theta_V, \chi)$ distributions (40)
Belle18-μ [21]	$\bar{B}^0 \to D^{*+}\mu^-\bar{\nu}$	$(w, \theta_\ell, \theta_V, \chi)$ distributions (40)
BR [18]	$\bar{B} \to D^{(*)}\ell\bar{\nu}$	branching ratios (2)
Lattice [32–34]	FFs $(f_{+,0}^{B\to D}, h_{A_1})$	Eqs. (3.10)–(3.12) constraints (7*)
LCSR [35]	FFs $(f_{+,0,T}^{B\to D}, A_{1,0}^{B\to D^*}, V^{B\to D^*}, T_{1,2,23}^{B\to D^*})$	Eqs. (3.13)–(3.21) constraints (33)
QCDSR [36–38]	FFs $(\hat{\chi}_{2,3}^{(n)}, \eta^{(n)})$	Eqs. (3.22)–(3.24) constraints (8)
UB [4]	U_{J^P}	Eqs. (3.25)–(3.28) constraints (4)

Table 1. Summary of the experimental data and the theory constraints used in our fit analysis. Numbers of independent data points are also exhibited in brackets. (*) The relation $f_+(q^2=0) = f_0(q^2=0)$ implies that the lattice result has only 6 independent observables.

Our fit procedure is briefly exhibited as follows. We basically take into account the full experimental data points of $\bar{B} \to D^{(*)}\ell\bar{\nu}$ and the applicable theoretical constraints on the specific FFs, as summarized in table 1. Namely, 184 data points are used to fit the free parameters. Regarding the theory constraints, we need to declare ways of treating uncertainties. First, we simply take them as normal distributions in order to obtain mean values and variances from the sampling points of the fitted parameters. As for the UBs, it is assumed such as, e.g., $(U_{0^+} - 0)^2/\chi_{0^+}(0)^2$. This means that 1σ deviation is the threshold for UB which should have to be satisfied in a final result. We will check this point later in section 3.4.4. After then, we will also discuss the QCDSR bounds on $\hat{\chi}_{2,3}^{(n)}$ and $\eta^{(n)}$ since they include special input of T and ω_0 (see appendix C for more detail) that have no fair description of "central value".[4]

For comparison and later discussion, we also consider the following case where limited data points are taken into account for a fit analysis: ***w*+theory** — only the w distributions along with the theory constraints and the branching ratios.

As for the phenomenological mode, we investigate SM, SM+V_2, SM+T, and SM+V_2+T as described in eq. (2.1) with the HQET parameterization for the FFs. Then we evaluate *Information Criterion* that offers the predictive accuracy of the model. To be precise, we employ cAIC defined as [25]

$$\mathrm{cAIC} = -2\ln\mathcal{L} + \frac{2k(k+1)}{n-k-1}\,, \tag{3.31}$$

where $\mathcal{L}$ is the maximum likelihood and n (k) denotes the number of data points (the model parameters to be fitted). The second term gives a penalty for overestimate of increasing number of model parameters. In our case, $k = 23 + 1(+1\,\text{or}\,+2)$ in the SM(+NP) for

[4]This issue might be similar for the LCSR bounds, but it is beyond the scope of the present work.

JHEP08(2020)006

NNLO (3/2/1), and similarly $k = 13+1(+1 \text{ or } +2)$ for (2/1/0), with $n = 184$. A preferred model has a smaller cAIC.

3.4 Result

First, we show our fit results of the HQET parameters and $|V_{cb}|$ for the SM(+NP) scenarios at the NNLO heavy quark expansion in table 2. We also evaluate how the present phenomenological models improve fit to data points by looking at difference in *Information Criterion* from a reference model. We define $\Delta\text{IC}_{\text{model}} = \text{cAIC}_0 - \text{cAIC}_{\text{model}}$, where $\text{cAIC}_0 = 987.4$ is the fit result of our reference model, SM NLO(3/2/–). We remark that a larger value of ΔIC implies a better improvement from the reference model. As seen from the result, all the present models improve the fit compared with the reference model in which $\hat{\ell}_i^{(n)} = 0$ is taken. This illustrates significance of non-zero values (beyond variances) for the NNLO parameters.

On the other hand, one finds that SM (2/1/0) is more preferred than SM (3/2/1). This is also similar to the cases of the SM + NP scenarios, whose details will be shown in the following subsection. This means that 23 HQET parameters in (3/2/1) are surplus to the present available experimental/theory 184 data points, and then 13 in (2/1/0) are sufficient to explain the available data points at present. However, we believe that this is not conclusive since it could vary as additional measurements become available in the future, e.g., by the Belle II experiment. Therefore, we still continue to examine the both cases of (2/1/0) and (3/2/1) in the following part of this work. For more details of our fit results, such as correlation matrix, see appendix D.

As a consistency check with integrated observables, we generate the branching ratios and the D^* polarization (e mode) that result in

$$\mathcal{B}(\bar{B}^0 \to D^+\ell^-\bar{\nu})_{\text{SM}} = \Big[(2.23 \pm 0.05)\%\,;\ (2.20 \pm 0.05)\%\Big]\,, \tag{3.32}$$

$$\mathcal{B}(\bar{B}^0 \to D^{*+}\ell^-\bar{\nu})_{\text{SM}} = \Big[(5.06 \pm 0.05)\%\,;\ (5.07 \pm 0.05)\%\Big]\,, \tag{3.33}$$

$$F_L^{D^*}(\bar{B}^0 \to D^{*+}e^-\bar{\nu})_{\text{SM}} = \Big[0.534 \pm 0.002\,;\ 0.531 \pm 0.002\Big]\,, \tag{3.34}$$

in the SM for the cases of $\big[(2/1/0);\ (3/2/1)\big]$, respectively. This is compared with the experimental measurements of $\mathcal{B}(\bar{B}^0 \to D^+\ell^-\bar{\nu})_{\text{exp}} = (2.31 \pm 0.03 \pm 0.09)\%$ and $\mathcal{B}(\bar{B}^0 \to D^{*+}\ell^-\bar{\nu})_{\text{exp}} = (5.06 \pm 0.02 \pm 0.12)\%$ from the world average [42], and $F_L^{D^*}(\bar{B}^0 \to D^{*+}e^-\bar{\nu})_{\text{exp}} = 0.56 \pm 0.02$ from ref. [43]. Note that $F_L^{D^*}(\bar{B}^0 \to D^{*+}e^-\bar{\nu})_{\text{exp}}$ is still preliminary (and thus we did not take it in our fit). We can see that they are in good agreements within uncertainties, but the best fit point for the D mode is a bit smaller than data, even though it was included in the fit.

3.4.1 $|V_{cb}|$ determination

Our fit results for $|V_{cb}|$ in the SM (2/1/0) and (3/2/1) scenarios are both close to the PDG combined average, $(39.5 \pm 0.9) \times 10^{-3}$, from the exclusive mode [18]. In table 3, we put summary for the recent $|V_{cb}|$ determinations along with the normalization factors $\mathcal{G}(1)$ and $\mathcal{F}(1)$.

JHEP08(2020)006

FF scenario	(3/2/1)		(2/1/0)			
Model	SM	SM+V_2	SM	SM+V_2	SM+T	SM+V_2 +T
$\lvert V_{cb}\rvert \times 10^3$	39.3 ± 0.6	39.9 ± 0.5	39.7 ± 0.6	39.9 ± 0.6	39.7 ± 0.6	39.9 ± 0.6
$C_{\rm NP}$	—	0.05 ± 0.01	—	0.02 ± 0.01	$\lvert 0.02 \pm 0.01\rvert$	$V_2 : 0.02 \pm 0.01$ $T : \lvert 0.02 \pm 0.01\rvert$
$\xi^{(1)}$	-0.93 ± 0.10	-0.94 ± 0.09	-1.10 ± 0.04	-1.09 ± 0.04	-1.09 ± 0.04	-1.09 ± 0.04
$\xi^{(2)}$	$+1.35 \pm 0.26$	$+1.37 \pm 0.25$	$+1.57 \pm 0.10$	$+1.55 \pm 0.10$	$+1.56 \pm 0.10$	$+1.54 \pm 0.10$
$\xi^{(3)}$	-2.67 ± 0.75	-2.71 ± 0.73	—	—	—	—
$\hat{\chi}_2^{(0)}$	-0.05 ± 0.02	-0.05 ± 0.02	-0.06 ± 0.02	-0.06 ± 0.02	-0.06 ± 0.02	-0.06 ± 0.02
$\hat{\chi}_2^{(1)}$	$+0.01 \pm 0.02$	$+0.01 \pm 0.02$	$+0.01 \pm 0.02$	$+0.01 \pm 0.02$	$+0.01 \pm 0.02$	$+0.00 \pm 0.02$
$\hat{\chi}_2^{(2)}$	-0.01 ± 0.02	-0.02 ± 0.02	—	—	—	—
$\hat{\chi}_3^{(1)}$	-0.05 ± 0.02	-0.05 ± 0.02	-0.03 ± 0.01	-0.04 ± 0.01	-0.03 ± 0.01	-0.04 ± 0.01
$\hat{\chi}_3^{(2)}$	-0.03 ± 0.03	$+0.01 \pm 0.03$	—	—	—	—
$\eta^{(0)}$	$+0.74 \pm 0.11$	$+0.71 \pm 0.11$	$+0.38 \pm 0.06$	$+0.37 \pm 0.06$	$+0.40 \pm 0.06$	$+0.38 \pm 0.06$
$\eta^{(1)}$	$+0.05 \pm 0.03$	$+0.05 \pm 0.03$	$+0.08 \pm 0.03$	$+0.08 \pm 0.03$	$+0.08 \pm 0.03$	$+0.07 \pm 0.03$
$\eta^{(2)}$	-0.05 ± 0.05	-0.06 ± 0.05	—	—	—	—
$\hat{\ell}_1^{(0)}$	$+0.09 \pm 0.18$	$+0.19 \pm 0.18$	$+0.50 \pm 0.16$	$+0.48 \pm 0.16$	$+0.50 \pm 0.16$	$+0.49 \pm 0.16$
$\hat{\ell}_1^{(1)}$	$+1.20 \pm 2.09$	-0.70 ± 1.92	—	—	—	—
$\hat{\ell}_2^{(0)}$	-2.29 ± 0.33	-1.64 ± 0.36	-2.16 ± 0.29	-1.93 ± 0.32	-2.24 ± 0.29	-2.00 ± 0.33
$\hat{\ell}_2^{(1)}$	-3.66 ± 1.56	-2.92 ± 1.55	—	—	—	—
$\hat{\ell}_3^{(0)}$	-1.90 ± 12.4	-1.50 ± 12.6	-1.14 ± 2.34	-0.23 ± 2.39	-1.21 ± 2.29	-0.32 ± 2.41
$\hat{\ell}_3^{(1)}$	$+3.91 \pm 4.35$	$+4.29 \pm 4.31$	—	—	—	—
$\hat{\ell}_4^{(0)}$	-2.56 ± 0.94	-2.22 ± 0.94	$+0.82 \pm 0.47$	$+0.97 \pm 0.48$	$+0.76 \pm 0.47$	$+0.94 \pm 0.49$
$\hat{\ell}_4^{(1)}$	$+1.78 \pm 0.93$	$+1.82 \pm 0.91$	—	—	—	—
$\hat{\ell}_5^{(0)}$	$+3.96 \pm 1.17$	$+6.31 \pm 1.32$	$+1.39 \pm 0.43$	$+2.03 \pm 0.59$	$+1.32 \pm 0.43$	$+1.99 \pm 0.59$
$\hat{\ell}_5^{(1)}$	$+2.10 \pm 1.47$	$+2.29 \pm 1.51$	—	—	—	—
$\hat{\ell}_6^{(0)}$	$+4.96 \pm 5.76$	$+7.15 \pm 5.87$	$+0.17 \pm 1.15$	$+0.90 \pm 1.23$	$+0.06 \pm 1.15$	$+0.81 \pm 1.24$
$\hat{\ell}_6^{(1)}$	$+5.08 \pm 2.97$	$+5.52 \pm 3.04$	—	—	—	—
ΔIC	118.1	128.4	162.4	161.5	161.3	160.4

Table 2. Fit results of the simultaneous determinations for the HQET parameters and $|V_{cb}|$ in several phenomenological models at NNLO with/without NP. Larger value of ΔIC indicates better improvement of the fit from the reference model of NLO(3/2/–).

Here we would like to discuss difference in the $|V_{cb}|$ determination between our results and one from ref. [17]. In their work, $|V_{cb}|$ has been extracted by using the fit result of the HQET parameters, and after then, by taking the integrated branching ratios of $\bar{B} \to D^{(*)}\ell\bar{\nu}$. Although the former fit analysis includes the experimental w distributions, it is utilized only to fit the HQET parameters. Indeed, we find that their result can be

JHEP08(2020)006

	all (2/1/0)	**all** (3/2/1)	PDG/HFLAV [18, 42]	***w*+theory** (3/2/1)	Ref. [17] (3/2/1)
$\lvert V_{cb}\rvert \times 10^3$	39.7 ± 0.6	39.3 ± 0.6	39.5 ± 0.9	40.3 ± 0.6	40.3 ± 0.8
$\mathcal{G}(1)$	1.044 ± 0.006	1.041 ± 0.006	1.054 ± 0.009	1.044 ± 0.006	—
$\mathcal{F}(1)$	0.900 ± 0.009	0.895 ± 0.011	0.904 ± 0.012	0.895 ± 0.011	—

Table 3. Comparison of the $|V_{cb}|$ determinations along with the normalization factors $\mathcal{F}(1)$ and $\mathcal{G}(1)$. In our work, these factors are simultaneously produced by the fit analysis.

reproduced when we perform the fit analysis with the data set of ***w*+theory** as shown in table 3. Therefore, we emphasize that the angular distributions are also significant for the $|V_{cb}|$ determination.

We also provide a fit result for $\mathcal{G}(w)$ and $\mathcal{F}(w)$ comparing them with those in the CLN parameterization. The traditional form of $\mathcal{G}(w)$ is expanded by z, with the coefficients by means of the slope parameter ρ^2, and with the assumption estimated by UB as in ref. [4]. In our study, we can directly produce the coefficients in z expansion, defined as

$$\mathcal{G}(w) \equiv \mathcal{G}(1) \sum_{n=0}^{3} g_n z^n \,, \tag{3.35}$$

with $g_0 = 1$. Our result is then

$$g_1 = -7.77 \pm 0.43 \,, \qquad g_2 = 24.9 \pm 5.3 \,, \qquad g_3 = -38.6 \pm 33.0 \,, \tag{3.36}$$

and $\mathcal{G}(1) = 1.041 \pm 0.006$ for SM (3/2/1), where the correlation matrix is put in appendix D. This is compared with the CLN form

$$g_1 = -8\rho^2 \,, \qquad g_2 = 51\rho^2 - 10 \,, \qquad g_3 = -252\rho^2 + 84 \,, \tag{3.37}$$

for $\rho^2 = 1.131 \pm 0.033$ [42]. One can see that our result has ~ 5 times larger uncertainties in the coefficients. This is mainly due to inclusion of larger number of the parameters to be fitted. Thus, our result is rather conservative than the simple approximation of CLN as expected. Also, keep the discussion around eq. (2.18) in mind when $\mathcal{G}(w)^2$ is calculated for the evaluation of the decay rate.

The CLN form for $\mathcal{F}(w)$ is constructed with $h_{A_1}(w)$, $R_1(w)$, and $R_2(w)$. As already explained, its CLN approximation is not appropriate for analyses with recent precise data. Instead, we provide the z expanded $\mathcal{F}(w)$ squared such as

$$\mathcal{F}(w)^2 \equiv \mathcal{F}(1)^2 \sum_{n=0}^{3} f_n^2 z^n \,, \tag{3.38}$$

with

$$\mathcal{F}(1) = 0.895 \pm 0.011 \,, \quad f_1^2 = -13.0 \pm 0.8 \,, \quad f_2^2 = 55.9 \pm 18.0 \,, \quad f_3^2 = -762 \pm 227 \,. \tag{3.39}$$

JHEP08(2020)006

3.4.2 NP scenarios

We have seen the fit results including the NP contributions in table 2. In the SM + T scenarios, our fit result indicates that the T contribution is constrained as $|C_T| < 0.025$ at 95% confidence level for the case of (3/2/1), which means zero-consistent, and hence omitted from the table. On the other hand, $|C_T| = 0.02 \pm 0.01$ is obtained for (2/1/0) as seen from the table, which implies that the best fit point favors non-zero T contribution although the uncertainty is still large. For both cases, the HQET parameters and $|V_{cb}|$ are then all consistent with those in the SM scenarios. This could be very interesting since the HQET parameterization model affects the fit result of the NP effect, and also the fit analysis has the NP sensitivity at the level of $\mathcal{O}(\%)$ of the SM value, $2\sqrt{2}G_F V_{cb}$.

The SM + V_2 scenarios also have the non-zero preferred value with the large uncertainty, $C_{V_2} = 0.05 \pm 0.01$ for (3/2/1) and $C_{V_2} = 0.02 \pm 0.01$ for (2/1/0). In addition, both cases give larger $|V_{cb}|$ than those in the SM, which would be interesting as it is different from the case for SM + T. Indeed, these changes improve the fit to the branching ratios. We obtain

$$\mathcal{B}(\bar{B}^0 \to D^+ \ell^- \bar{\nu})_{\mathrm{SM}+V_2} = \Big[(2.29 \pm 0.06)\%\,;\ (2.33 \pm 0.06)\%\Big]\,, \tag{3.40}$$

$$\mathcal{B}(\bar{B}^0 \to D^{*+} \ell^- \bar{\nu})_{\mathrm{SM}+V_2} = \Big[(5.05 \pm 0.05)\%\,;\ (5.03 \pm 0.05)\%\Big]\,, \tag{3.41}$$

for SM + V_2 $\big[(2/1/0); (3/2/1)\big]$ from the fit result. Thus we can see that the branching ratios are in perfect agreements with the experimental measurements.

The SM + V_2 + T scenarios provide us with the most general model-independent fits. The (3/2/1) case however results in the same as that of SM + V_2, inherited from the zero-consistent SM + T result for C_T, and hence omitted from the table. The (2/1/0) case finds non-zero best fit points for C_{V_2} and C_T by slightly changing the HQET parameters from the other scenarios. In this case, we obtain $\mathcal{B}(\bar{B}^0 \to D^+ \ell^- \bar{\nu})_{\mathrm{SM}+V_2+T} = (2.29 \pm 0.06)\%$ and $\mathcal{B}(\bar{B}^0 \to D^{*+} \ell^- \bar{\nu})_{\mathrm{SM}+V_2+T} = (5.02 \pm 0.05)\%$.

The SM+NP fit improvements ΔIC for (2/1/0) are a bit lower than the SM fit because of the additional degree, C_X. On the other hand, SM + V_2 (3/2/1) has a clear improvement compared with SM (3/2/1).

In figure 1 (top), we show preferred regions of $|V_{cb}|$ and C_X in the SM + NP scenarios, where the regions in blue, green, and gray are favored in the SM + V_2(3/2/1), SM + V_2(2/1/0), and SM + T(2/1/0) scenarios, respectively. We also include the allowed region from the inclusive process for SM + NP as depicted in the yellow region. It can be derived with the use of refs. [16, 44, 45], in which discrepancy of the $|V_{cb}|$ determination among the exclusive and inclusive processes has been investigated. Then, it is found that our fit result loosens the deviation in the SM + V_2 and SM + T scenarios, but it is still not in a sufficient agreement. Lastly, one can see that the SM + V_2 + T scenario, displayed with the dashed lines, has no impact on this issue.

A corresponding LHC bound on C_X is naively obtained by the following discussion. These days LHC constraints on NP effects have been getting severer. In ref. [46], the authors have shown that τ searches with high p_T at 36 fb^{-1} [47, 48] give an upper limit on the WCs

JHEP08(2020)006

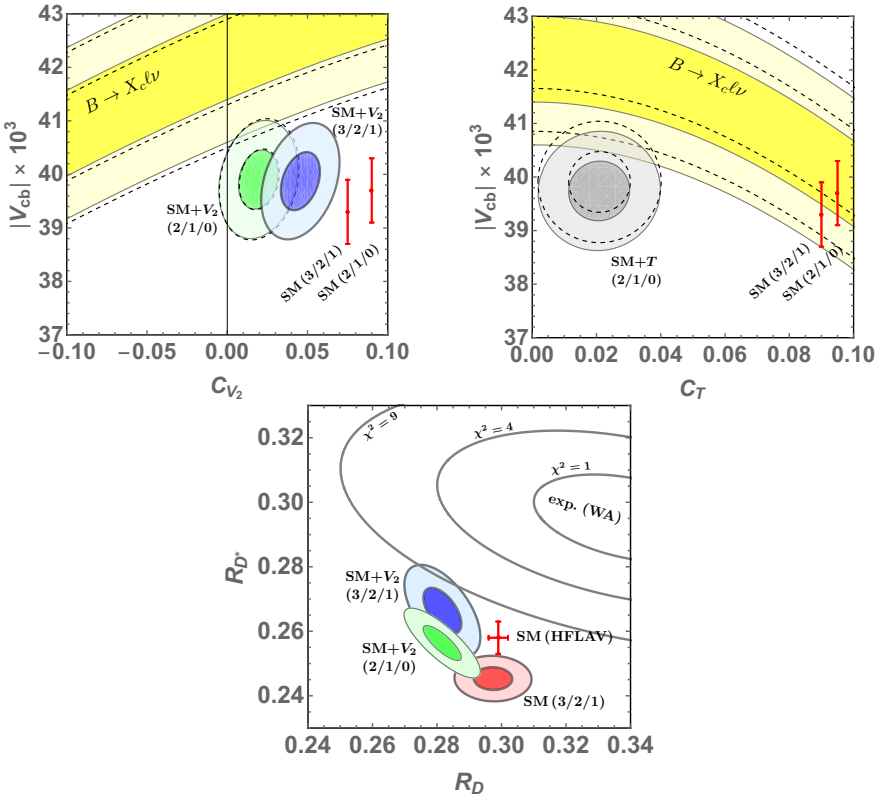

Figure 1. [Top] Preferred regions of C_X and $|V_{cb}|$ in the SM + NP scenarios. The regions in blue, green, and gray are favored in the SM + $V_2(3/2/1)$, SM + $V_2(2/1/0)$, and SM + $T(2/1/0)$ scenarios, respectively. The yellow band indicates the allowed region from the inclusive mode. The contour lines correspond to $\Delta\chi^2 = 1, 4$. The red bars are the SM results for $|V_{cb}|$. The dashed lines are the case for SM + V_2 + T by fixing another NP contribution to be $C_T = 0.05$ and $C_{V_2} = 0.02$ in the left and right panels, respectively. [Bottom] Contour plot for predictions on R_D and R_{D^*} in the SM(+NP) scenarios, where the regions for SM(3/2/1), SM + $V_2(3/2/1)$, and SM + $V_2(2/1/0)$ are shown in red, blue, and green, respectively. The combined experimental result (gray solid curves that correspond to $\Delta\chi^2 = 1, 4, 9$) and the SM prediction in the literature (red bar) are taken from ref. [42].

for the $b \to c\tau\nu$ current. (See, also refs. [49–53] in the context of NP interpretations of the $R_{D^{(*)}}$ anomaly.) Similarly, e and μ searches with high p_T at 139 fb^{-1} [54] give an upper limit on C_X defined as in eq. (2.1). Comparing those experimental constraints in looking at a tail of the m_T plane (~ 1.4 TeV), we have the naive estimate of the upper bound as $|C_{V_2}| \lesssim 0.1$ and $|C_T| \lesssim 0.05$. Therefore, our fit result of $C_X \sim \mathcal{O}(0.01)$ is in the region of interest also for the LHC search. A further study of the LHC bound in higher p_T ranges is work in progress.

3.4.3 Observables for $\bar{B} \to D^{(*)}\tau\bar{\nu}$

With the CLN parameterization, SM predictions and/or NP investigations have been provided with respect to $\bar{B} \to D^{(*)}\tau\bar{\nu}$ in the literature, (e.g., see refs. [55, 56] for recent works), since the experimental results have shown significant deviations from the SM predictions in

JHEP08(2020)006

	R_D	R_{D^*}	P_τ^D	$P_\tau^{D^*}$	$F_L^{D^*}$
SM (2/1/0)	0.289 ± 0.004	0.248 ± 0.001	0.331 ± 0.004	-0.496 ± 0.007	0.464 ± 0.003
SM (3/2/1)	0.297 ± 0.006	0.245 ± 0.004	0.326 ± 0.003	-0.503 ± 0.020	0.460 ± 0.008
SM (HFLAV [42])	0.299 ± 0.003	0.258 ± 0.005	—	—	—
SM (ref. [17])	0.297 ± 0.003	0.250 ± 0.003	0.321 ± 0.003	-0.496 ± 0.015	0.464 ± 0.010
SM + V_2 (2/1/0)	0.282 ± 0.006	0.256 ± 0.005	0.332 ± 0.004	-0.499 ± 0.007	0.465 ± 0.003
LFU case	0.292 ± 0.004	0.247 ± 0.001	0.332 ± 0.004	-0.499 ± 0.007	0.463 ± 0.003
SM + V_2 (3/2/1)	0.282 ± 0.006	0.266 ± 0.007	0.329 ± 0.003	-0.506 ± 0.020	0.464 ± 0.008
LFU case	0.309 ± 0.006	0.244 ± 0.004	0.329 ± 0.003	-0.507 ± 0.020	0.460 ± 0.008

Table 4. Predictions of the $\bar{B} \to D^{(*)}\tau\bar{\nu}$ observables.

the measurements of the ratios: $R_D = 0.340 \pm 0.027 \pm 0.013$ and $R_{D^*} = 0.295 \pm 0.011 \pm 0.008$ (combined average in ref. [42]). In recent years, challenging measurements of the τ and D^* polarizations in $\bar{B} \to D^*\tau\bar{\nu}$ have also been reported as $P_\tau^{D^*} = -0.38 \pm 0.51\,^{+0.21}_{-0.16}$ [57] and $F_L^{D^*} = 0.60 \pm 0.08 \pm 0.04$ [43].

Here, we also investigate these $\bar{B} \to D^{(*)}\tau\bar{\nu}$ observables with the use of our fit results in the SM(+NP) scenarios of the HQET parameterization. Note that, in this work, we mainly consider NP contributions only to the (e, μ) modes. Namely, the denominators of the ratios $R_{D^{(*)}}$ are only affected by the NP contribution. In this sense, our NP investigation has a different view from numerous previous studies for the $R_{D^{(*)}}$ anomaly, e.g., see refs. [58–60] for the case of the HQET parameterization. Also note that we take the proper $\epsilon_{a,b,c}$ expansion for these observables.

In table 4, we list our predictions on the $\bar{B} \to D^{(*)}\tau\bar{\nu}$ observables in the present models, along with those from refs. [17, 42]. Our analysis shows that the SM(2/1/0) predicts smaller values for both R_D and R_{D^*} than those of the HFLAV report. On the other hand, the SM(3/2/1) has the consistent value for R_D while smaller for R_{D^*}. This is a similar behavior with that obtained in ref. [17]. Then, it is also found that the polarizations for (3/2/1) are consistent with the reference. We obtain the same results for the cases of SM + T.

The SM + V_2 models give $R_{D^{(*)}}$ different from the SM predictions, which could be NP signals at the Belle II experiment with large statistics. To be precise, both cases point to the R_D and R_{D^*} values smaller and larger than the SM predictions, respectively. In particular, it is interesting that the R_{D^*} deviation from the measurement becomes smaller for SM + V_2(3/2/1). This is a key feature for this model. However, we have to remark that the experimental measurement for $R_{D^{(*)}}$ is analyzed by means of both τ and (e, μ) distributions subtracted from background. The present measurement is then done with the assumption that the (e, μ) modes obey the SM. Thus, in the presence of NP in the (e, μ) modes, re-analysis is needed by taking the NP effect. Although such a NP effect of $\mathcal{O}(\%)$ is negligible for the present analysis, it could become significant as larger number of events are accumulated at the Belle II experiment.

Predicted values of the tau observables in the SM + V_2 + T scenarios are all equivalent to those in SM + V_2 within the present uncertainties.

JHEP08(2020)006

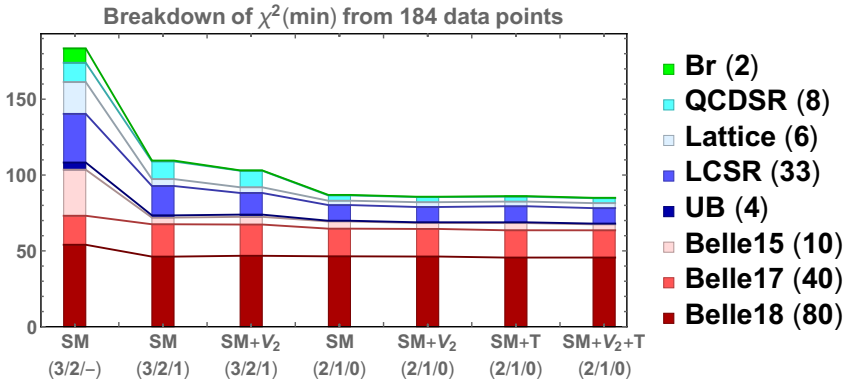

Figure 2. The breakdown of the χ^2 deviations at our best fit results from the 184 data points.

Finally, we show a summary plot for the predictions on R_D and R_{D^*} in the SM(+NP) scenarios in figure 1 (bottom), where the allowed regions for SM(3/2/1), SM + V_2(3/2/1), and SM + V_2(2/1/0) are shown in red, blue, and green, respectively. The combined experimental result (gray curves) and the referred SM prediction (red bar) are taken from ref. [42].

One might be interested in the case where the NP contribution is universal for all the leptons (LFU), such that $C_X^e = C_X^\mu = C_X^\tau$. We also show predictions for such a case in the table. For SM + V_2, $(1 \pm C_{V_2})^2$ enters as the overall factor both in the numerator and denominator of R_D/R_{D^*}, and thus the values should be equivalent to the SM ones if using the same inputs for the HQET parameters. (To be precise, R_{D^*} is affected by C_{V_2} beyond the overall factor, but such an effect is quite small.) Our V_2 LFU results are not the same as our SM values due to the differences in the fitted HQET parameters which can be seen in table 2. In particular, the (3/2/1) model predicts larger R_D than the other cases and scenarios, which could be interesting. We also found that T LFU results are all similar to the corresponding SM values. In any event, however, our results show a fact that the present $R_{D^{(*)}}$ anomaly is not resolved by the LFU type NP contribution. Therefore, some large C_X^τ violating LFU is necessary.

3.4.4 Theoretical uncertainty

For the present analyses so far, we have treated the theory constraints as being normally distributed for simplicity and in order to obtain the applicable outputs. Thanks to it, we can display the breakdown of the χ^2 deviations for our fit results as in figure 2.

The UBs are taken as the Gaussian distribution assuming the central value as zero while the standard deviation as the calculated upper limit given in eqs. (3.25)–(3.28). We have checked the breakdown of the χ^2 deviation from the UBs for all the present models considered in our analysis and then have confirmed that those for the UBs are all within 1σ.

As for the bounds from QCDSR, we have derived the constraints of eqs. (3.22)–(3.24) and again taken as normal distributions. Our fit results, however, show that some of the NLO parameters are deviated from these constraints as seen in table 2. In particular, our MCMC run finds the best fit point of $\hat{\chi}_3^{(1)} \sim \mathcal{O}(-0.01)$ that has a large deviation from the

JHEP08(2020)006

QCDSR constraint $\sim \mathcal{O}(+0.01)$. Indeed, the χ^2 breakdown for the QCDSR constraints is $\chi^2_{\rm QCDSR} \sim 10(4)$ for the SM (3/2/1) (SM (2/1/0)). To see its effect, we test a fit analysis where possible ranges for the NLO parameters, $\hat{\chi}^{(n)}_{2,3}$ and $\eta^{(n)}$, are restricted as in eqs. (3.22)–(3.24). Then we find that the outputs of $|V_{cb}|$ and the LO parameters $\xi^{(n)}$ are not much affected while those of the NNLO parameters $\hat{\ell}^{(n)}_i$ are shifted, compared with the results obtained in table 2. In this case, however, the NLO parameter fits have bad convergences and their distributions are far away from the normal distributions. Also, we have checked that the observables such as the branching ratios are all consistent. In this sense, we can say that our main conclusion is not affected by this issue.

4 Summary

We have investigated the semi-leptonic decays of $\bar{B} \to D^{(*)}\ell\bar{\nu}$ in terms of the HQET parameterization for the form factors, with the heavy quark expansion up to $\mathcal{O}(1/m_c^2)$, and beyond the simple approximation considered in the original CLN parameterization. It is given with the $z = (\sqrt{w+1} - \sqrt{2})/(\sqrt{w+1} + \sqrt{2})$ expanded form, and then the highest order for the expansion is in principle arbitrary. In our work, we have followed the models from ref. [17] denoted as (2/1/0) and (3/2/1) for the z expansions in the (leading/subleading/subsub-leading) IW functions.

The analysis with this setup was first given in ref. [17], and then we have extended it to the comprehensive analyses including (i) simultaneous fit of $|V_{cb}|$ and the HQET parameters to the available experimental full distribution data and the theory constraints, and (ii) NP contributions of the V_2 and T types, such as $(\bar{c}\gamma^\mu P_R b)(\bar{\ell}\gamma_\mu P_L \nu_\ell)$ and $(\bar{c}\sigma^{\mu\nu} P_L b)(\bar{\ell}\sigma_{\mu\nu} P_L \nu_\ell)$, to the decay distributions and rates. For this purpose, we have performed the Bayesian fit analyses by using `Stan` program, a state-of-the-art public platform for statistical computation, in which MCMC runs with various algorithms are possible.

Then it has been shown that our $|V_{cb}|$ fit results for the SM (2/1/0) and (3/2/1) scenarios are both close to the PDG combined average, $(39.5 \pm 0.9) \times 10^{-3}$, from the exclusive mode:

$$|V_{cb}|_{(2/1/0)} = (39.7 \pm 0.6) \times 10^{-3}\,, \tag{4.1}$$

$$|V_{cb}|_{(3/2/1)} = (39.3 \pm 0.6) \times 10^{-3}\,, \tag{4.2}$$

as also summarized in table 3. This implies that the deviation from the inclusive mode still holds. We have also found that the fit to the w distribution data with the theory constraints (***w*+theory**) reproduce the larger $|V_{cb}|$ value completely consistent with that reported in ref. [17]. This could imply significance of the angular distribution data for $\bar{B} \to D^*\ell\bar{\nu}$. Besides, we have evaluated *Information Criterion* to see how the inclusion of the $\mathcal{O}(1/m_c^2)$ parameters improve the fit. Then we see that the 23 HQET parameters of (3/2/1) are surplus while 13 of (2/1/0) are sufficient for the statistical modeling to explain the present available data points.

The SM + NP scenarios have been studied with the same manner. At first, we have confirmed that SM+T(3/2/1) is constrained as $|C_T| < 0.025$ at 95% confidence level and the

JHEP08(2020)006

best fit point is zero-consistent. On the other hand, it has turned out that SM + $T(2/1/0)$ is allowed to have non-zero contribution, $|C_T| = 0.02 \pm 0.01$, to the processes. This could be very interesting since the HQET parameterization model affects the fit result of the NP effect. Furthermore, a significant point is that the fit analysis has the NP sensitivity at the level of $\mathcal{O}(\%)$.

Then, we have also obtained non-zero preferred values in the SM + V_2 scenarios as $C_{V_2} = 0.05 \pm 0.01$ for $(3/2/1)$ and $C_{V_2} = 0.02 \pm 0.01$ for $(2/1/0)$. *Information Criterion* also suggests that SM + V_2 is favored at the same level with the SM scenarios. In addition, both cases give larger $|V_{cb}|$ than those in the SM, but they are still not in a sufficient agreement with the $|V_{cb}|$ determination from the inclusive process. In turn, we have considered SM + $V_2 + T$ for the model-independent fit. We then found that C_T is zero-consistent and the result is the same as that of SM+V_2 for the $(3/2/1)$ scenario. The $(2/1/0)$ scenario points to non-zero C_{V_2} and C_T with the same $|V_{cb}|$ as that of SM+V_2. This is summarized in figure 1 (top). The applicable LHC bound is naively given as $|C_{V_2}| \lesssim 0.1$ and $|C_T| \lesssim 0.05$ estimated from the m_T plane at $\sim 1.4\,\text{TeV}$ and thus a further LHC search would be interesting.

Finally, we have produced our predictions on the $\bar{B} \to D^{(*)}\tau\bar{\nu}$ observables in the present models. It is summarized in table 4 and figure 1 (bottom). Our prediction in SM$(2/1/0)$ has smaller values for both R_D and R_{D^*} comapred with those in the HFLAV report. On the other hand, SM$(3/2/1)$ predicts the consistent value for R_D while smaller for R_{D^*}. In the SM+V_2 scenarios, NP only contributes to the light-lepton modes and then it results in the R_D and R_{D^*} values smaller and larger than the SM predictions, respectively. It is also seen that the R_{D^*} deviation from the experimental measurement becomes milder ($\sim 1.9\sigma$) than the one in the SM. This is a key feature for this model derived from our fit analysis. Quantitatively, we have 4.24σ and 3.66σ significances for the $R_{D^{(*)}}$ deviation in SM $(2/1/0)$ and $(3/2/1)$, respectively. This is compared with 3.03σ in SM (HFLAV) assuming no correlation. As for SM + V_2, we see 3.76σ $(2/1/0)$ and 2.96σ $(3/2/1)$. For a specific interest, we have checked the case where the NP contribution is lepton-flavor universal, $C_X^e = C_X^\mu = C_X^\tau$ for the tau observables. Then we saw that SM+$V_2(3/2/1)$ with LFU predicts larger R_D value (0.309 ± 0.06) than any other models and scenarios, which could be interesting.

For the present analyses, we have treated the theory constraints as being normally distributed for simplicity and in order to obtain the applicable outputs. A further practical treatment on the theoretical uncertainties could be possible, for instance, when we implement this work in the public `HEPfit` package [61]. We leave it for our future work.

We conclude from this work that the available full distribution data of $\bar{B} \to D^{(*)}\ell\bar{\nu}$ has potential to fit a large number of the parameters in the HQET parameterization together with $|V_{cb}|$, and a further improvement is expected at the Belle II experiment. The fit analysis also has the NP sensitivity with the $\mathcal{O}(\%)$ level of the SM contribution, and then it could be examined with the $\bar{B} \to D^{(*)}\tau\bar{\nu}$ observables in future. Interesting directions of future work are, for example, CP violation [62] and QED corrections [63] in the $\bar{B} \to D^{(*)}\ell\bar{\nu}$ distributions with respect to the HQET parameterization.

JHEP08(2020)006

Acknowledgments

We are grateful to Martin Jung for useful comments on the HQET parameterization. We thank Minoru Tanaka for discussion about QCDSR. RW thanks Vincent Picaud for helpful suggestions on the usage of `MathematicaStan`. RW also thanks Marco Ciuchini for discussion on MCMC. SI is grateful to Kazuhiro Tobe for discussion about various aspects of this work. SI also thanks Kodai Matsuoka and Noritsugu Tsuzuki for useful comments on the experimental measurements of $\bar{B} \to D^{(*)}\ell\bar{\nu}$ and $\bar{B} \to D^{(*)}\tau\bar{\nu}$. We also thank Nagoya University Theoretical Elementary Particle Physics Laboratory for providing computational resources. The work of SI is supported by the Japan Society for the Promotion of Science (JSPS) Research Fellowships for Young Scientists, No. 19J10980 and Core to Core Program, No. JPJSCCA20200002.

A α_s and $1/m_Q$ corrections

Here we list functions for the α_s and $1/m_{b,c}$ corrections. We have followed the analytic result from ref. [8]. The α_s corrections, $\delta\hat{h}_{X,\alpha_s}$, are given as

$$\begin{aligned}
\delta\hat{h}_{+,\alpha_s} = \frac{1}{6z_{cb}^2(w-w_{cb})^2}\big[&4z_{cb}^2(w-w_{cb})^2\Omega_w(w)+(w+1)\big(-1+(w+w^2+2w_{cb})(z_{cb}^2+1)z_{cb}\\
&+2(w^2-w(2+3w_{cb})+w_{cb})z_{cb}^2-z_{cb}^4\big)r_w(w)\\
&+(w_{cb}-w)\big(1+w+w(10+z_{cb})z_{cb}+(-2-12w_{cb}+z_{cb})z_{cb}\big)z_{cb}\\
&-(1+w_{cb}-w-w^2)(1-z_{cb}^2)z_{cb}\log z_{cb}\big]+V(\mu)\,, \qquad \text{(A.1)}\\
\delta\hat{h}_{-,\alpha_s} = \frac{1+w}{6z_{cb}^2(w-w_{cb})^2}\big[&-\big(1+(1-2w-w^2)z_{cb}+z_{cb}^2\big)(1-z_{cb}^2)r_w(w)-(w-w_{cb})(1-z_{cb}^2)z_{cb}\\
&-\big(2(1+z_{cb}+z_{cb}^2)-w(1+4z_{cb}+z_{cb}^2)\big)z_{cb}\log z_{cb}\big]\,, \qquad \text{(A.2)}\\
\delta\hat{h}_{V,\alpha_s} = \frac{1}{6z_{cb}(w-w_{cb})}\big[&4z_{cb}(w-w_{cb})\Omega_w(w)+2(w+1)((3w-1)z_{cb}-z_{cb}^2-1)r_w(w)\\
&-12z_{cb}(w-w_{cb})-(z_{cb}^2-1)\log z_{cb}\big]+V(\mu)\,, \qquad \text{(A.3)}\\
\delta\hat{h}_{A_1,\alpha_s} = \frac{1}{6z_{cb}(w-w_{cb})}\big[&4z_{cb}(w-w_{cb})\Omega_w(w)+2(w-1)((3w+1)z_{cb}-z_{cb}^2-1)r_w(w)\\
&-12z_{cb}(w-w_{cb})-(z_{cb}^2-1)\log z_{cb}\big]+V(\mu)\,, \qquad \text{(A.4)}\\
\delta\hat{h}_{A_2,\alpha_s} = \frac{1}{6z_{cb}^2(w-w_{cb})^2}\big[&\big(2+(2w^2-5w-1)z_{cb}+2w(2w-1)z_{cb}^2+(1-w)z_{cb}^3\big)\,r_w(w)\\
&-2z_{cb}(z_{cb}+1)(w-w_{cb})+(z_{cb}^2-(4w+2)z_{cb}+3+2w)z_{cb}\log z_{cb}\big]\,, \qquad \text{(A.5)}\\
\delta\hat{h}_{A_3,\alpha_s} = \frac{1}{6z_{cb}(w-w_{cb})^2}\big[&4(w-w_{cb})^2z_{cb}\Omega_w(w)+\big(1+w-2w^2+6w^3z_{cb}+z_{cb}^2(-1+2z_{cb})\\
&-wz_{cb}(4+3z_{cb})-2(-1+w)(-1+z_{cb}+3wz_{cb}-z_{cb}^2)w_{cb}\big)r_w(w)\\
&-2wz_{cb}(1+6w+z_{cb})+(-10+24w+2z_{cb})z_{cb}w_{cb}\\
&+(-2+w+(2+4w)z_{cb}-(2+3w)z_{cb}^2)\log z_{cb}\big]+V(\mu)\,, \qquad \text{(A.6)}
\end{aligned}$$

JHEP08(2020)006

$$\delta\hat{h}_{S,\alpha_s} = \frac{1}{3z_{cb}(w-w_{cb})}\left[2z_{cb}(w-w_{cb})\Omega_w(w)-(w-1)(z_{cb}+1)^2 r_w(w)\right.$$
$$\left.+(z_{cb}^2-1)\log z_{cb}\right]+S(\mu)\,, \tag{A.7}$$

$$\delta\hat{h}_{P,\alpha_s} = \frac{1}{3z_{cb}(w-w_{cb})}\left[2z_{cb}(w-w_{cb})\Omega_w(w)-(w+1)(z_{cb}-1)^2 r_w(w)\right.$$
$$\left.+(z_{cb}^2-1)\log z_{cb}\right]+S(\mu)\,, \tag{A.8}$$

$$\delta\hat{h}_{T,\alpha_s} = \frac{1}{3z_{cb}(w-w_{cb})}\left[2z_{cb}(w-w_{cb})\Omega_w(w)+\left(4z_{cb}w^2-(1-z_{cb})^2 w-(1+z_{cb})^2\right)r_w(w)\right.$$
$$\left.-6z_{cb}(w-w_{cb})+(1-z_{cb}^2)\log z_{cb}\right]+T(\mu)\,, \tag{A.9}$$

$$\delta\hat{h}_{T_1,\alpha_s} = \frac{1}{3z_{cb}(w-w_{cb})}\left[2z_{cb}(w-w_{cb})\Omega_w(w)+2z_{cb}(w^2-1)r_w(w)\right.$$
$$\left.-6z_{cb}(w-w_{cb})+(1-z_{cb}^2)\log z_{cb}\right]+T(\mu)\,, \tag{A.10}$$

$$\delta\hat{h}_{T_2,\alpha_s} = \frac{w+1}{3z_{cb}(w-w_{cb})}\left[(1-z_{cb}^2)r_w(w)+2z_{cb}\log z_{cb}\right]\,, \tag{A.11}$$

$$\delta\hat{h}_{T_3,\alpha_s} = \frac{1}{3z_{cb}(w-w_{cb})}\left[(z_{cb}w-1)r_w(w)-z_{cb}\log z_{cb}\right]\,, \tag{A.12}$$

with

$$z_{cb} = \frac{m_c}{m_b}\,,\quad w_{cb} = \frac{1}{2}\left(z_{cb}+z_{cb}^{-1}\right)\,,\quad w_\pm(w) = w\pm\sqrt{w^2-1}\,, \tag{A.13}$$

$$r_w(w) = \frac{\log w_+(w)}{\sqrt{w^2-1}}\,, \tag{A.14}$$

$$\Omega_w(w) = \frac{w}{2\sqrt{w^2-1}}\Big[2\mathrm{Li}_2(1-w_-(w)z_{cb})-2\mathrm{Li}_2(1-w_+(w)z_{cb})$$
$$+\mathrm{Li}_2(1-w_+^2(w))-\mathrm{Li}_2(1-w_-^2(w))\Big]-wr_w(w)\log z_{cb}+1\,, \tag{A.15}$$

where $\mathrm{Li}_2(x)=\int_x^0 dt\log(1-t)/t$ is dilogarithmical function. The above results are obtained at the scale $\mu_{\sqrt{bc}}=\sqrt{m_b m_c}$, namely $V(\mu_{\sqrt{bc}})=S(\mu_{\sqrt{bc}})=T(\mu_{\sqrt{bc}})=0$. Otherwise, the scale factors are given as

$$V(\mu) = -\frac{2}{3}\left(wr_w(w)-1\right)\log\frac{m_b m_c}{\mu^2}\,, \tag{A.16}$$

$$S(\mu) = -\frac{1}{3}\left(2wr_w(w)+1\right)\log\frac{m_b m_c}{\mu^2}\,, \tag{A.17}$$

$$T(\mu) = -\frac{1}{3}\left(2wr_w(w)-3\right)\log\frac{m_b m_c}{\mu^2}\,. \tag{A.18}$$

Note that we set the scale as $\mu_b = 4.2\,\mathrm{GeV}$ in our analysis.

The $1/m_{b,c}$ corrections involve four sub-leading IW functions, $\chi_{1\text{-}3}(w)$ and $\xi_3(w)$, one of which (usually χ_1) can be absorbed into the definition of $\xi(w)$. For the form of $\delta\hat{h}_{X,m_{b,c}}$, the sub-leading IW functions divided by $\xi(w)$ are defined as in eq. (2.11). Following ref. [8],

JHEP08(2020)006

we can write $\delta\hat{h}_{X,m_{b,c}}$ as

$$\delta\hat{h}_{+,m_b} = \delta\hat{h}_{+,m_c} = \delta\hat{h}_{T_1,m_b} = -4(w-1)\hat{\chi}_2(w) + 12\hat{\chi}_3(w)\,, \tag{A.19}$$

$$\delta\hat{h}_{-,m_b} = -\delta\hat{h}_{-,m_c} = \delta\hat{h}_{T_2,m_b} = 1 - 2\eta(w)\,, \tag{A.20}$$

$$\begin{aligned}\delta\hat{h}_{V,m_b} &= \delta\hat{h}_{A_3,m_b} = \delta\hat{h}_{P,m_b} = \delta\hat{h}_{T,m_b} = \delta\hat{h}_{T,m_c} \\ &= 1 - 2\eta(w) - 4(w-1)\hat{\chi}_2(w) + 12\hat{\chi}_3(w)\,,\end{aligned} \tag{A.21}$$

$$\delta\hat{h}_{V,m_c} = 1 - 4\hat{\chi}_3(w)\,, \tag{A.22}$$

$$\begin{aligned}\delta\hat{h}_{A_1,m_b} &= \delta\hat{h}_{S,m_b} = \delta\hat{h}_{S,m_c} \\ &= (w-1)\Big[(w+1)^{-1}\big(1-2\eta(w)\big) - 4\hat{\chi}_2(w)\Big] + 12\hat{\chi}_3(w)\,,\end{aligned} \tag{A.23}$$

$$\delta\hat{h}_{A_1,m_c} = (w-1)(w+1)^{-1} - 4\hat{\chi}_3(w)\,, \tag{A.24}$$

$$\delta\hat{h}_{A_2,m_b} = \delta\hat{h}_{T_3,m_b} = 0\,, \tag{A.25}$$

$$\delta\hat{h}_{A_2,m_c} = -2(w+1)^{-1}\big(1+\eta(w)\big) + 4\hat{\chi}_2(w)\,, \tag{A.26}$$

$$\delta\hat{h}_{A_3,m_c} = 1 - 2(w+1)^{-1}\big(1+\eta(w)\big) - 4\hat{\chi}_2(w) - 4\hat{\chi}_3(w)\,, \tag{A.27}$$

$$\delta\hat{h}_{P,m_c} = -1 + 2\big(1+\eta(w)\big) + 4(w-1)\hat{\chi}_2(w) - 4\hat{\chi}_3(w)\,, \tag{A.28}$$

$$\delta\hat{h}_{T_1,m_c} = -4\hat{\chi}_3(w)\,, \tag{A.29}$$

$$\delta\hat{h}_{T_2,m_c} = -1\,, \tag{A.30}$$

$$\delta\hat{h}_{T_3,m_c} = (w+1)^{-1}\big(1+\eta(w)\big) + 2\hat{\chi}_2(w)\,, \tag{A.31}$$

where $\chi_1(w)$ is absorbed.

The $1/m_c^2$ corrections consist of six subsub-leading IW functions $\ell_{1\text{–}6}(w)$ in the absence of the $1/m_b^2$ and $1/(m_b m_c)$ corrections [26]. The expressions for $\delta\hat{h}_{X,m_c^2}$ can be obtained from ref. [26] as

$$\delta\hat{h}_{+,m_c^2} = \hat{\ell}_1(w)\,, \tag{A.32}$$

$$\delta\hat{h}_{-,m_c^2} = \hat{\ell}_4(w)\,, \tag{A.33}$$

$$\delta\hat{h}_{V,m_c^2} = \hat{\ell}_2(w) - \hat{\ell}_5(w)\,, \tag{A.34}$$

$$\delta\hat{h}_{A_1,m_c^2} = \hat{\ell}_2(w) - \frac{w-1}{w+1}\hat{\ell}_5(w)\,, \tag{A.35}$$

$$\delta\hat{h}_{A_2,m_c^2} = \hat{\ell}_3(w) + \hat{\ell}_6(w)\,, \tag{A.36}$$

$$\delta\hat{h}_{A_3,m_c^2} = \hat{\ell}_2(w) - \hat{\ell}_3(w) - \hat{\ell}_5(w) + \hat{\ell}_6(w)\,, \tag{A.37}$$

$$\delta\hat{h}_{S,m_c^2} = \hat{\ell}_1(w) - \frac{w-1}{w+1}\hat{\ell}_4(w)\,, \tag{A.38}$$

$$\delta\hat{h}_{P,m_c^2} = \hat{\ell}_2(w) + (w-1)\hat{\ell}_3(w) + \hat{\ell}_5(w) - \hat{\ell}_6(w)\,, \tag{A.39}$$

$$\delta\hat{h}_{T,m_c^2} = \hat{\ell}_1(w) - \hat{\ell}_4(w)\,, \tag{A.40}$$

$$\delta\hat{h}_{T_1,m_c^2} = \hat{\ell}_2(w)\,, \tag{A.41}$$

JHEP08(2020)006

$$\delta\hat{h}_{T_2,m_c^2} = \hat{\ell}_5(w)\,, \tag{A.42}$$

$$\delta\hat{h}_{T_3,m_c^2} = \frac{1}{2}\big(\hat{\ell}_3(w) - \hat{\ell}_6(w)\big)\,, \tag{A.43}$$

for $\hat{\ell}(w) = \ell(w)/\xi(w)$.

B Angular dependence

Here we derive the full angular distribution of eqs. (2.24) and (2.25). In the SM, the squared decay amplitude of $\mathcal{M}$ for $B^0 \to D^{*-}\ell\bar{\nu}$, followed by $D^{*-} \to \bar{D}^0\pi^-$, can be represented as

$$|\mathcal{M}(q^2,\theta_\ell,\theta_V,\chi)|^2 = \left|\sum_{\lambda_{D^*},\lambda'_{D^*}} \mathcal{S}^{\lambda_{D^*}}(\theta_\ell)\,\mathcal{D}^1_{\lambda_{D^*},\lambda'_{D^*}}(\chi)\,\mathcal{T}^{\lambda'_{D^*}}(\theta_V)\right|^2, \tag{B.1}$$

where

$$\mathcal{S}^{\lambda_{D^*}}(q^2,\theta_\ell) = \frac{G_F}{\sqrt{2}}V_{cb}\sum_{\lambda_W} H^{\lambda_{D^*}}_{\lambda_W} L^{\lambda_\ell=-1/2}_{\lambda_W}\,, \tag{B.2}$$

shows the usual helicity amplitude for $B^0 \to D^{*-}\ell\bar{\nu}$, which has been described in ref. [29], whereas $\mathcal{T}^{\lambda'_{D^*}}(\theta_V)$ indicates the amplitude for $D^{*-} \to \bar{D}^0\pi^-$ and $\mathcal{D}^1_{\lambda_{D^*}\,\lambda'_{D^*}}(\chi)$ is the Wigner rotation that connects two decay planes defined for θ_ℓ (ℓ–ν plane at W rest frame) and θ_V (D–π plane at D^* rest frame). Then the latter two can be obtained as

$$\mathcal{T}^0 = \frac{N}{2}\frac{3}{\pi}\cos\theta_V\,, \quad \mathcal{T}^{\pm1} = \mp\frac{N}{2}\frac{3}{2\pi}\sin\theta_V\,, \tag{B.3}$$

and

$$\mathcal{D}^1_{0,0} = 1\,, \quad \mathcal{D}^1_{\pm1,\pm1} = e^{\pm i\chi}\,, \quad \text{others} = 0\,, \tag{B.4}$$

where the normalization factor N is determined so that

$$\int_{-1}^{1} d\cos\theta_V \int_{-\pi}^{\pi} d\chi \frac{d\Gamma_{\text{full}}}{dw\,d\cos\theta_\ell\,d\cos\theta_V\,d\chi} = \frac{d\Gamma(B^0\to D^{*-}\ell\bar{\nu})}{dw\,d\cos\theta_\ell}\mathcal{B}(D^{*-}\to\bar{D}^0\pi^-)\,, \tag{B.5}$$

is satisfied. Following $L^{\lambda_\ell=-1/2}_{\lambda_W}$ by substituting $\theta_\tau = \pi - \theta_\ell$ (due to difference in definition) given in ref. [29] along with the above description, we can derive the SM contribution in eqs. (2.24) and (2.25). Note that we have defined $H^\pm_\pm \equiv H_\pm(w)$ and $H^0_0 \equiv H_0(w)$ in the main text. The angular dependence for the case of the V_2 type operator is given simply by replacing $H_\pm(w) \to -C_{V_2}H_\mp(w)$ and $H_0(w) \to -C_{V_2}H_0(w)$.

As for the tensor NP operator, a similar procedure is applicable to obtain the angular distribution by taking

$$\mathcal{S}^{\lambda_{D^*}}(q^2,\theta_\ell) = \frac{2G_F}{\sqrt{2}}V_{cb}C_T\sum_{\lambda,\lambda'} H^{\lambda_{D^*}}_{\lambda,\lambda'} L^{\lambda_\ell=+1/2}_{\lambda,\lambda'}\,, \tag{B.6}$$

where L is again described in ref. [29], $H^\pm_{\pm,0} = \pm H^\pm_{\pm,s} \equiv H^T_\pm(w)$, and $H^0_{+,-} = H^0_{0,s} \equiv H^T_0(w)$. Since the lepton helicity of the tensor current is flipped compared with the SM current, one finds that the SM and tensor operators have no interference.

JHEP08(2020)006

C Constraints from QCDSR

The sub-leading IW functions, $\chi_{2,3}(w)$, $\eta(w)$, have been investigated by introducing QCDSR analysis up to two-loop perturbative corrections in the literature [36–38]. In this approach, they are described as

$$\chi_i(w) = [\alpha_s(1\,\mathrm{GeV})]^{1/3}\,\bar{\chi}_i(w)\,, \qquad \eta(w) = \frac{1}{3} + \Delta(w)\,, \tag{C.1}$$

with

$$\begin{aligned}
\bar{\chi}_2(w)\left[F^2\bar{\Lambda}e^{-2\bar{\Lambda}/T}\right] &= -\frac{\alpha_s T^4}{8\pi^3}\left(\frac{2}{w+1}\right)^2\left(\frac{1-r(w)}{w-1}+2\right)\delta_3\left(\frac{\omega_0}{T}\right) \\
&\quad + \frac{\alpha_s T\langle\bar{q}q\rangle}{6\pi}\left(\frac{1-r(w)}{w-1}+\frac{1}{w+1}\right)\delta_0\left(\frac{\omega_0}{T}\right) - \frac{\langle\alpha_s GG\rangle}{96\pi}\frac{2}{w+1}\,,
\end{aligned} \tag{C.2}$$

$$\begin{aligned}
\bar{\chi}_3(w)\left[F^2\bar{\Lambda}e^{-2\bar{\Lambda}/T}\right] &= \frac{\alpha_s T^4}{8\pi^3}\left(\frac{2}{w+1}\right)^2\left(wr(w)-1+\ln\frac{w+1}{2}\right)\delta_3\left(\frac{\omega_0}{T}\right) \\
&\quad + \frac{3\delta\omega_2}{32\pi^2}\omega_0^3 e^{-\omega_0/T}\left[\left(\frac{2}{w+1}\right)^2 - \xi(w)\right] \\
&\quad + \frac{\alpha_s T\langle\bar{q}q\rangle}{6\pi}\left[2-r(w)-\xi(w)\right]\delta_0\left(\frac{\omega_0}{T}\right) \\
&\quad + \frac{\langle\alpha_s GG\rangle}{96\pi}\left[\frac{2}{w+1}-\xi(w)\right] - \frac{\langle\bar{q}g_s\sigma_{\mu\nu}G^{\mu\nu}q\rangle}{48T}\left[1-\xi(w)\right],
\end{aligned} \tag{C.3}$$

$$\begin{aligned}
\Delta(w)\left[\xi(w)F^2\bar{\Lambda}e^{-2\bar{\Lambda}/T}\right] &= \frac{\alpha_s T^4}{12\pi^3}\left(\frac{2}{w+1}\right)^2\left(11+6w+(3+w)r(w)\right)\delta_3\left(\frac{\omega_0}{T}\right) \\
&\quad - \frac{2\alpha_s T\langle\bar{q}q\rangle}{9\pi}\left(7+(3-w)r(w)\right)\delta_0\left(\frac{\omega_0}{T}\right) \\
&\quad + \frac{\langle\alpha_s GG\rangle}{72\pi}\frac{w-1}{w+1} + \frac{\langle\bar{q}g_s\sigma_{\mu\nu}G^{\mu\nu}q\rangle}{18T}(w-1)\,,
\end{aligned} \tag{C.4}$$

where

$$r(w) = \frac{1}{\sqrt{w^2-1}}\ln(w+\sqrt{w^2-1})\,, \qquad \delta_n(x) = \frac{1}{\Gamma(n+1)}\int_0^x dz z^n e^{-z}\,. \tag{C.5}$$

The continuum threshold ω_0 and Borel parameter T control stability of the sum rule, as will be explained below. The renormalized factor $[\alpha_s(1\,\mathrm{GeV})]^{1/3}$ connects the sub-leading IW functions in QCD $\bar{\chi}_i(w)$ to our basis $\chi_i(w)$.

The prefactors, presented with $\left[\cdots\right]$ in eqs. (C.3)–(C.5), contain the leading IW function $\xi(w)$, heavy meson decay constant F (HQET basis), and heavy quark-meson mass difference $\bar{\Lambda}$. From two-current correlator, one finds

$$F^2\bar{\Lambda}e^{-2\bar{\Lambda}/T} = \frac{9T^4}{8\pi^2}\delta_3\!\left(\frac{\omega_0}{T}\right) - \frac{\langle\bar{q}g_s\sigma_{\mu\nu}G^{\mu\nu}q\rangle}{4T}\,, \qquad \text{(see ref. [36])} \tag{C.6}$$

$$\xi(w)F^2\bar{\Lambda}e^{-2\bar{\Lambda}/T} = \frac{9T^4}{8\pi^2}\left(\frac{2}{1+w}\right)^2\delta_3\!\left(\frac{\omega_0}{T}\right) - \frac{2w+1}{3}\frac{\langle\bar{q}g_s\sigma_{\mu\nu}G^{\mu\nu}q\rangle}{4T}\,, \qquad \text{(see ref. [38])} \tag{C.7}$$

JHEP08(2020)006

while $\xi(w)$ can be independently obtained as [37]

$$\xi(w) = \frac{K(T,\omega_0,w)}{K(T,\omega_0,1)}, \quad \Big(\text{equivalently } \xi(w)F^2 e^{-2\bar{\Lambda}/T} = K(T,\omega_0,w)\,,\Big)$$
$$K(T,\omega_0,w) = \frac{3T^3}{4\pi^2}\left(\frac{2}{1+w}\right)^2 \delta_2\!\left(\frac{\omega_0}{T}\right) - \langle\bar{q}q\rangle + \frac{2w+1}{3}\frac{\langle\bar{q}g_s\sigma_{\mu\nu}G^{\mu\nu}q\rangle}{4T^2}\,. \tag{C.8}$$

Note that $-\frac{1}{2}\frac{\partial}{\partial T^{-1}}K(T,\omega_0,w)$ equals to r.h.s. of eq. (C.7) and hence these expressions are consistent with each other.

Input parameters for the QCDSR predictions consist of the decay constant $F = (0.3\pm0.05)\,\text{GeV}^{3/2}$ [36], the mass difference $\bar{\Lambda} = (0.5\pm0.07)\,\text{GeV}$ [36], the spin-symmetry-violating correction $\delta\omega_2 = (-0.1\pm0.02)\,\text{GeV}$ only for $\chi_3(w)$ [37], and the following vacuum condensates:

$$\langle\bar{q}q\rangle = -(0.25\pm0.01\,\text{GeV})^3\,, \qquad \text{(from refs. [64–66])} \tag{C.9}$$
$$\langle\alpha_s GG\rangle = (6.35\pm0.35)\times10^{-2}\,\text{GeV}^4\,, \qquad \text{(from ref. [67])} \tag{C.10}$$
$$\langle\bar{q}g_s\sigma_{\mu\nu}G^{\mu\nu}q\rangle = m_0^2\langle\bar{q}q\rangle \;\text{ with }\; m_0^2 = (0.8\pm0.2)\,\text{GeV}^2 \qquad \text{(from refs. [68–70])}\,. \tag{C.11}$$

The continuum threshold ω_0 and the Borel parameter T have been determined in the literature so that $\bar{\chi}_{2,3}(1)$ and $\Delta(1)$ are stabilized. In our case, concerning higher derivatives such as $\hat{\chi}_{2,3}^{(2)}$ and $\eta^{(2)}$, we take

$$0.7\,\text{GeV} < T < 1\,\text{GeV}\,, \quad 1.7\,\text{GeV} < \omega_0 < 2.3\,\text{GeV}\,. \tag{C.12}$$

Substituting QCDSR for F and $\bar{\Lambda}$ as in eqs. (C.6) and (C.8), and then taking numerical input within 1σ uncertainties, we obtain the constraints as in eqs. (3.22)–(3.24) of the main text. Note that $\hat{\chi}_i(w) = \chi(w)/\xi(w)$ and we take the conservative ranges for the uncertainties, which is in agreement with ref. [8].

D Fit results with some details

Here we write down useful output data obtained by our fit analyses. First, we show correlation among our fit results of the HQET parameters, for SM (3/2/1) in tables 5–8, and for SM (2/1/0) in tables 9–12.

We then provide our fit results of $\mathcal{G}(w)$ and $\mathcal{F}(w)$ for SM (3/2/1) with the z expansion forms as defined in eqs. (3.35) and (3.38):

$$\text{corr.}(\mathcal{G}) = \begin{pmatrix} 1.0000 & -0.4626 & 0.2962 & -0.1886 \\ -0.4626 & 1.0000 & -0.7231 & 0.4812 \\ 0.2962 & -0.7231 & 1.0000 & -0.9278 \\ -0.1886 & 0.4812 & -0.9278 & 1.0000 \end{pmatrix}, \tag{D.1}$$

for $(\mathcal{G}(1), g_1, g_2, g_3)$ and

$$\text{corr.}(\mathcal{F}^2) = \begin{pmatrix} 1.0000 & -0.2661 & 0.1328 & -0.2465 \\ -0.2661 & 1.0000 & -0.8456 & 0.8270 \\ 0.1328 & -0.8456 & 1.0000 & -0.8367 \\ -0.2465 & 0.8270 & -0.8367 & 1.0000 \end{pmatrix}, \tag{D.2}$$

JHEP08(2020)006

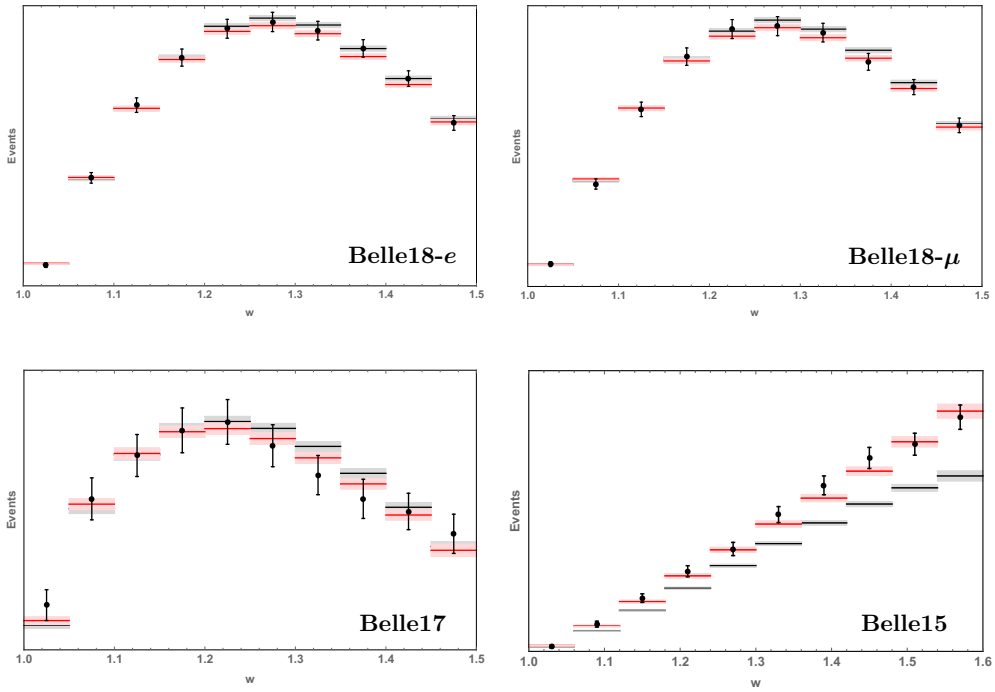

Figure 3. Binned decay distributions with respect to w with the comparisons between data and the fit results from the SM (2/1/0) [red] and SM (3/2/–) [gray] scenarios.

for $(\mathcal{F}(1), f_1^2, f_2^2, f_3^2)$. In turn, R_D–R_{D^*} correlations are obtained as -0.15, -0.03, -0.81, and -0.57 for SM (2/1/0), SM (3/2/1), SM+V_2 (2/1/0), and SM+V_2 (3/2/1), respectively.

In figures 3–6, we also show the binned decay distributions with respect to $(w, \cos\theta_\ell, \cos\theta_V, \chi)$ with the comparisons between data and the fit results in the SM (2/1/0) [red] and SM (3/2/–) [gray] scenarios, in order to visualize the improvement on the fits. Note that the distributions for Belle17 (Belle18) are those of the decay rates (folded signal events) as explained in the main text.

JHEP08(2020)006

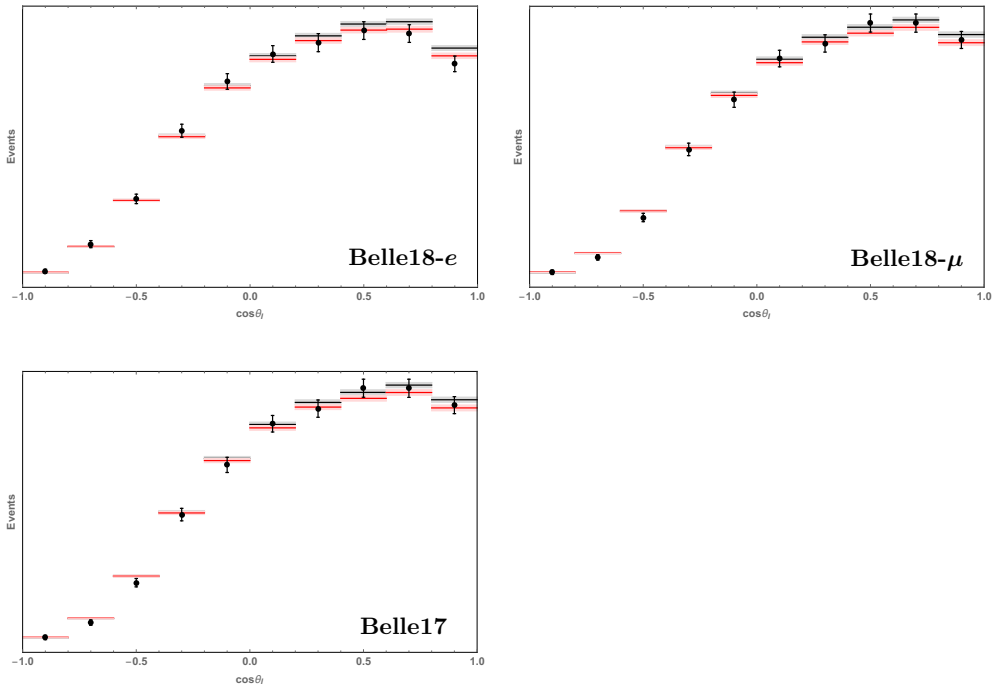

Figure 4. Binned decay distributions of $\cos\theta_\ell$. Conventions are the same as in figure 3.

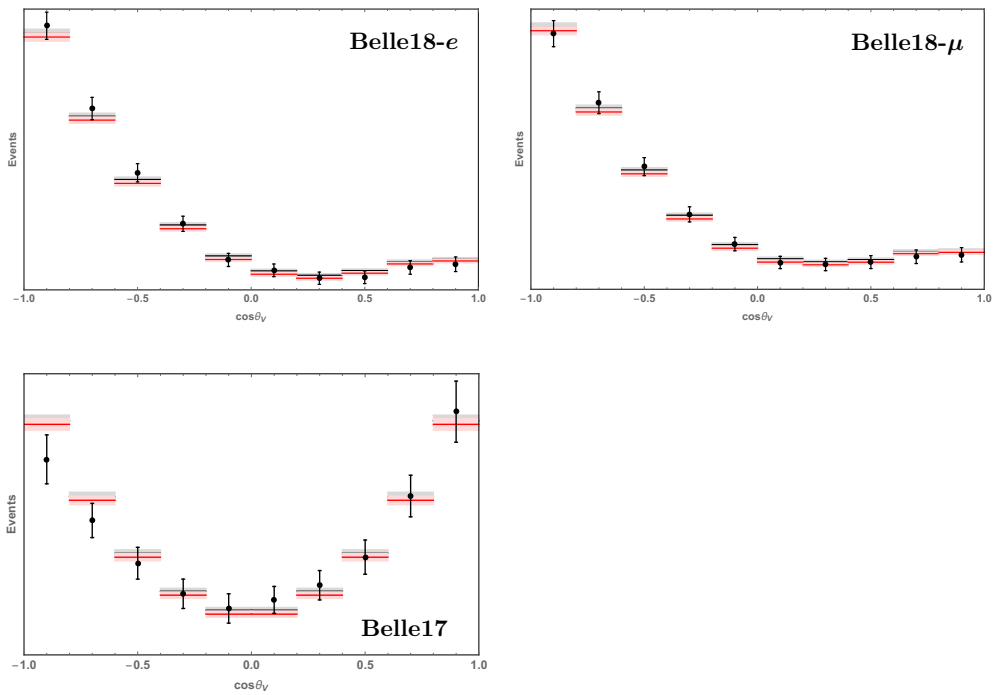

Figure 5. Binned decay distributions of $\cos\theta_V$. Conventions are the same as in figure 3.

JHEP08(2020)006

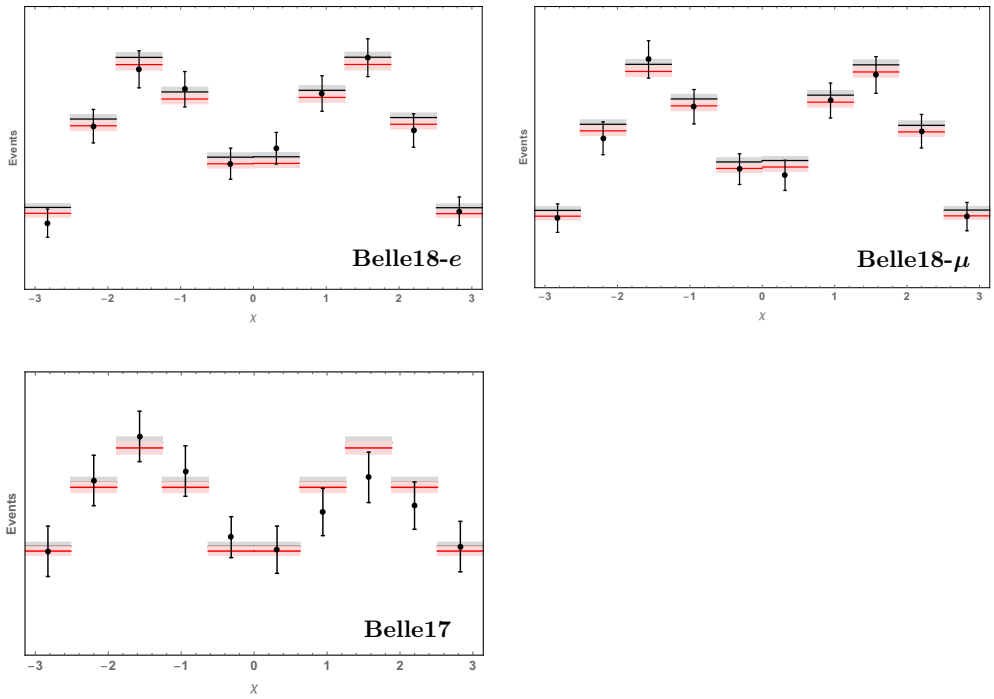

Figure 6. Binned decay distributions of χ. Conventions are the same as in figure 3.

corr.	$\lvert V_{cb}\rvert$	$\xi^{(1)}$	$\xi^{(2)}$	$\xi^{(3)}$	$\hat{\chi}_2^{(0)}$	$\hat{\chi}_2^{(1)}$	$\hat{\chi}_2^{(2)}$	$\hat{\chi}_3^{(1)}$	$\hat{\chi}_3^{(2)}$	$\eta^{(0)}$	$\eta^{(1)}$	$\eta^{(2)}$
$\lvert V_{cb}\rvert$	1.0000	0.2807	−0.2096	0.1785	0.0058	−0.0621	−0.0691	0.0005	0.3333	0.0014	−0.0078	−0.0188
$\xi^{(1)}$	0.2807	1.0000	−0.9295	0.8577	0.1694	−0.0862	0.0192	−0.0947	0.3637	0.2613	0.0261	0.0178
$\xi^{(2)}$	−0.2096	−0.9295	1.0000	−0.9851	−0.1760	0.0975	−0.0187	0.0263	−0.3641	−0.2324	−0.0129	−0.0160
$\xi^{(3)}$	0.1785	0.8577	−0.9851	1.0000	0.1718	−0.0964	0.0223	0.0055	0.3351	0.2088	0.0062	0.0149
$\hat{\chi}_2^{(0)}$	0.0058	0.1694	−0.1760	0.1718	1.0000	−0.0185	−0.0183	0.0484	0.0573	0.0518	0.0123	−0.0248
$\hat{\chi}_2^{(1)}$	−0.0621	−0.0862	0.0975	−0.0964	−0.0185	1.0000	−0.0089	0.0772	0.1369	−0.0068	−0.0258	−0.0069
$\hat{\chi}_2^{(2)}$	−0.0691	0.0192	−0.0187	0.0223	−0.0183	−0.0089	1.0000	−0.0124	0.3396	0.0213	−0.0065	−0.0676
$\hat{\chi}_3^{(1)}$	0.0005	−0.0947	0.0263	0.0055	0.0484	0.0772	−0.0124	1.0000	0.0404	−0.0400	0.0234	0.0454
$\hat{\chi}_3^{(2)}$	0.3333	0.3637	−0.3641	0.3351	0.0573	0.1369	0.3396	0.0404	1.0000	0.1322	0.0241	0.1332
$\eta^{(0)}$	0.0014	0.2613	−0.2324	0.2088	0.0518	−0.0068	0.0213	−0.0400	0.1322	1.0000	−0.0141	−0.0440
$\eta^{(1)}$	−0.0078	0.0261	−0.0129	0.0062	0.0123	−0.0258	−0.0065	0.0234	0.0241	−0.0141	1.0000	−0.0284
$\eta^{(2)}$	−0.0188	0.0178	−0.0160	0.0149	−0.0248	−0.0069	−0.0676	0.0454	0.1332	−0.0440	−0.0284	1.0000

Table 5. Correlation among $\left\{\xi^{(n)}, \hat{\chi}_{2,3}^{(n)}, \eta^{(n)}\right\}$–$\left\{\xi^{(n)}, \hat{\chi}_{2,3}^{(n)}, \eta^{(n)}\right\}$ in SM (3/2/1).

JHEP08(2020)006

corr.	$\hat{\ell}_1^{(0)}$	$\hat{\ell}_1^{(1)}$	$\hat{\ell}_2^{(0)}$	$\hat{\ell}_2^{(1)}$	$\hat{\ell}_3^{(0)}$	$\hat{\ell}_3^{(1)}$	$\hat{\ell}_4^{(0)}$	$\hat{\ell}_4^{(1)}$	$\hat{\ell}_5^{(0)}$	$\hat{\ell}_5^{(1)}$	$\hat{\ell}_6^{(0)}$	$\hat{\ell}_6^{(1)}$
$\lvert V_{cb}\rvert$	0.0143	−0.4568	−0.7995	−0.3826	−0.0109	−0.0820	0.0246	0.0660	0.3028	−0.1854	0.0598	−0.1803
$\xi^{(1)}$	−0.3296	−0.8549	−0.3734	−0.9066	−0.0298	−0.2690	−0.2662	0.0900	0.0388	−0.1974	0.0921	−0.5075
$\xi^{(2)}$	0.3352	0.7655	0.3288	0.7709	0.0303	0.2386	0.2505	−0.1322	−0.0630	0.2526	−0.0827	0.4896
$\xi^{(3)}$	−0.3226	−0.6930	−0.3006	−0.6834	−0.0304	−0.2152	−0.2314	0.1472	0.0664	−0.2617	0.0729	−0.4596
$\hat{\chi}_2^{(0)}$	−0.0134	0.0542	−0.0332	−0.0655	−0.0019	−0.0449	−0.0507	0.0232	0.0009	−0.0194	0.0496	−0.0113
$\hat{\chi}_2^{(1)}$	0.0032	0.0622	0.0642	0.0880	−0.0176	−0.0209	−0.0041	−0.0177	−0.0041	0.0030	−0.0217	0.0338
$\hat{\chi}_2^{(2)}$	0.0102	−0.0512	0.0418	0.0106	0.0334	−0.0758	−0.0243	−0.0036	−0.0041	0.0018	0.0340	−0.0372
$\hat{\chi}_3^{(1)}$	−0.3001	−0.1324	0.0115	0.1256	−0.0060	0.0255	0.0343	0.0233	0.0174	−0.0224	−0.0167	0.0381
$\hat{\chi}_3^{(2)}$	0.0308	−0.6003	−0.3223	−0.3126	0.0186	−0.1419	−0.1426	0.0792	0.1145	−0.1497	0.0824	−0.2139
$\eta^{(0)}$	−0.0999	−0.1983	−0.0952	−0.1839	0.0083	0.0928	−0.8842	−0.5828	−0.3765	0.0521	0.1033	0.1541
$\eta^{(1)}$	0.0029	−0.0396	0.0008	−0.0338	−0.0111	−0.0108	0.0046	−0.1132	−0.0309	0.0033	−0.0085	−0.0061
$\eta^{(2)}$	0.0418	−0.1045	0.0136	−0.0221	−0.0069	−0.0516	0.0687	−0.2907	0.0036	−0.0178	−0.0135	−0.0342

Table 6. Correlation among $\left\{\xi^{(n)},\, \hat{\chi}_{2,3}^{(n)},\, \eta^{(n)}\right\}$–$\left\{\hat{\ell}_{1\text{–}6}^{(n)}\right\}$ in SM (3/2/1).

corr.	$\lvert V_{cb}\rvert$	$\xi^{(1)}$	$\xi^{(2)}$	$\xi^{(3)}$	$\hat{\chi}_2^{(0)}$	$\hat{\chi}_2^{(1)}$	$\hat{\chi}_2^{(2)}$	$\hat{\chi}_3^{(1)}$	$\hat{\chi}_3^{(2)}$	$\eta^{(0)}$	$\eta^{(1)}$	$\eta^{(2)}$
$\hat{\ell}_1^{(0)}$	0.0143	−0.3296	0.3352	−0.3226	−0.0134	0.0032	0.0102	−0.3001	0.0308	−0.0999	0.0029	0.0418
$\hat{\ell}_1^{(1)}$	−0.4568	−0.8549	0.7655	−0.6930	0.0542	0.0622	−0.0512	−0.1324	−0.6003	−0.1983	−0.0396	−0.1045
$\hat{\ell}_2^{(0)}$	−0.7995	−0.3734	0.3288	−0.3006	−0.0332	0.0642	0.0418	0.0115	−0.3223	−0.0952	0.0008	0.0136
$\hat{\ell}_2^{(1)}$	−0.3826	−0.9066	0.7709	−0.6834	−0.0655	0.0880	0.0106	0.1256	−0.3126	−0.1839	−0.0338	−0.0221
$\hat{\ell}_3^{(0)}$	−0.0109	−0.0298	0.0303	−0.0304	−0.0019	−0.0176	0.0334	−0.0060	0.0186	0.0083	−0.0111	−0.0069
$\hat{\ell}_3^{(1)}$	−0.0820	−0.2690	0.2386	−0.2152	−0.0449	−0.0209	−0.0758	0.0255	−0.1419	0.0928	−0.0108	−0.0516
$\hat{\ell}_4^{(0)}$	0.0246	−0.2662	0.2505	−0.2314	−0.0507	−0.0041	−0.0243	0.0343	−0.1426	−0.8842	0.0046	0.0687
$\hat{\ell}_4^{(1)}$	0.0660	0.0900	−0.1322	0.1472	0.0232	−0.0177	−0.0036	0.0233	0.0792	−0.5828	−0.1132	−0.2907
$\hat{\ell}_5^{(0)}$	0.3028	0.0388	−0.0630	0.0664	0.0009	−0.0041	−0.0041	0.0174	0.1145	−0.3765	−0.0309	0.0036
$\hat{\ell}_5^{(1)}$	−0.1854	−0.1974	0.2526	−0.2617	−0.0194	0.0030	0.0018	−0.0224	−0.1497	0.0521	0.0033	−0.0178
$\hat{\ell}_6^{(0)}$	0.0598	0.0921	−0.0827	0.0729	0.0496	−0.0217	0.0340	−0.0167	0.0824	0.1033	−0.0085	−0.0135
$\hat{\ell}_6^{(1)}$	−0.1803	−0.5075	0.4896	−0.4596	−0.0113	0.0338	−0.0372	0.0381	−0.2139	0.1541	−0.0061	−0.0342

Table 7. Correlation among $\left\{\hat{\ell}_{1\text{–}6}^{(n)}\right\}$–$\left\{\xi^{(n)},\, \hat{\chi}_{2,3}^{(n)},\, \eta^{(n)}\right\}$ in SM (3/2/1).

JHEP08(2020)006

corr.	$\hat{\ell}_1^{(0)}$	$\hat{\ell}_1^{(1)}$	$\hat{\ell}_2^{(0)}$	$\hat{\ell}_2^{(1)}$	$\hat{\ell}_3^{(0)}$	$\hat{\ell}_3^{(1)}$	$\hat{\ell}_4^{(0)}$	$\hat{\ell}_4^{(1)}$	$\hat{\ell}_5^{(0)}$	$\hat{\ell}_5^{(1)}$	$\hat{\ell}_6^{(0)}$	$\hat{\ell}_6^{(1)}$
$\hat{\ell}_1^{(0)}$	1.0000	0.2371	0.0446	0.2740	0.0343	0.0668	0.3403	−0.1619	0.0205	0.0542	−0.0009	0.1550
$\hat{\ell}_1^{(1)}$	0.2371	1.0000	0.4762	0.8234	0.0194	0.2486	0.1900	0.0097	−0.1005	0.1966	−0.0863	0.4662
$\hat{\ell}_2^{(0)}$	0.0446	0.4762	1.0000	0.3309	0.0141	−0.0389	0.0715	−0.0389	−0.0603	0.0155	−0.0258	0.0183
$\hat{\ell}_2^{(1)}$	0.2740	0.8234	0.3309	1.0000	0.0690	0.3588	0.1839	−0.0939	−0.0263	0.3067	−0.0342	0.6221
$\hat{\ell}_3^{(0)}$	0.0343	0.0194	0.0141	0.0690	1.0000	−0.5168	−0.0007	−0.0067	0.0591	0.0560	0.9787	−0.2958
$\hat{\ell}_3^{(1)}$	0.0668	0.2486	−0.0389	0.3588	−0.5168	1.0000	−0.0759	−0.1192	−0.1505	0.3221	−0.5437	0.8919
$\hat{\ell}_4^{(0)}$	0.3403	0.1900	0.0715	0.1839	−0.0007	−0.0759	1.0000	0.4221	0.3323	−0.0423	−0.0880	−0.1174
$\hat{\ell}_4^{(1)}$	−0.1619	0.0097	−0.0389	−0.0939	−0.0067	−0.1192	0.4221	1.0000	0.2675	−0.1021	−0.0360	−0.2420
$\hat{\ell}_5^{(0)}$	0.0205	−0.1005	−0.0603	−0.0263	0.0591	−0.1505	0.3323	0.2675	1.0000	−0.5833	0.1354	−0.2695
$\hat{\ell}_5^{(1)}$	0.0542	0.1966	0.0155	0.3067	0.0560	0.3221	−0.0423	−0.1021	−0.5833	1.0000	−0.0022	0.5301
$\hat{\ell}_6^{(0)}$	−0.0009	−0.0863	−0.0258	−0.0342	0.9787	−0.5437	−0.0880	−0.0360	0.1354	−0.0022	1.0000	−0.3591
$\hat{\ell}_6^{(1)}$	0.1550	0.4662	0.0183	0.6221	−0.2958	0.8919	−0.1174	−0.2420	−0.2695	0.5301	−0.3591	1.0000

Table 8. Correlation among $\left\{\hat{\ell}_{1\text{–}6}^{(n)}\right\}$–$\left\{\hat{\ell}_{1\text{–}6}^{(n)}\right\}$ in SM (3/2/1).

corr.	$\lvert V_{cb}\rvert$	$\xi^{(1)}$	$\xi^{(2)}$	$\hat{\chi}_2^{(0)}$	$\hat{\chi}_2^{(1)}$	$\hat{\chi}_3^{(1)}$	$\eta^{(0)}$	$\eta^{(1)}$
$\lvert V_{cb}\rvert$	1.0000	0.1002	0.1283	−0.0494	−0.0594	−0.4822	−0.2104	−0.0876
$\xi^{(1)}$	0.1002	1.0000	−0.9012	0.3099	0.0193	−0.1968	−0.0321	0.0926
$\xi^{(2)}$	0.1283	−0.9012	1.0000	−0.3127	0.1381	−0.0625	0.0350	−0.0639
$\hat{\chi}_2^{(0)}$	−0.0494	0.3099	−0.3127	1.0000	0.0962	0.0604	−0.2061	0.0025
$\hat{\chi}_2^{(1)}$	−0.0594	0.0193	0.1381	0.0962	1.0000	0.3050	0.0147	−0.1087
$\hat{\chi}_3^{(1)}$	−0.4822	−0.1968	−0.0625	0.0604	0.3050	1.0000	−0.2991	−0.0072
$\eta^{(0)}$	−0.2104	−0.0321	0.0350	−0.2061	0.0147	−0.2991	1.0000	0.2309
$\eta^{(1)}$	−0.0876	0.0926	−0.0639	0.0025	−0.1087	−0.0072	0.2309	1.0000

Table 9. Correlation among $\left\{\xi^{(n)}, \hat{\chi}_{2,3}^{(n)}, \eta^{(n)}\right\}$–$\left\{\xi^{(n)}, \hat{\chi}_{2,3}^{(n)}, \eta^{(n)}\right\}$ in SM (2/1/0).

JHEP08(2020)006

corr.	$\hat{\ell}_1^{(0)}$	$\hat{\ell}_2^{(0)}$	$\hat{\ell}_3^{(0)}$	$\hat{\ell}_4^{(0)}$	$\hat{\ell}_5^{(0)}$	$\hat{\ell}_6^{(0)}$
$\lvert V_{cb}\rvert$	−0.0096	−0.8276	0.0225	0.2246	0.1837	0.0306
$\xi^{(1)}$	−0.3082	−0.4799	0.0183	0.0420	0.3977	0.1684
$\xi^{(2)}$	0.3377	0.2386	−0.0229	−0.0162	−0.2336	−0.1027
$\hat{\chi}_2^{(0)}$	0.0696	−0.0604	−0.0291	0.1489	0.0896	0.0323
$\hat{\chi}_2^{(1)}$	−0.0916	0.0459	−0.1991	0.0255	0.1137	−0.0848
$\hat{\chi}_3^{(1)}$	−0.3307	0.5291	−0.1191	0.2770	−0.1426	−0.1737
$\eta^{(0)}$	0.2129	0.0913	−0.0119	−0.6829	−0.3207	0.0029
$\eta^{(1)}$	−0.1483	0.0151	−0.0307	−0.3803	−0.0484	0.0398

Table 10. Correlation among $\left\{\xi^{(n)},\, \hat{\chi}_{2,3}^{(n)},\, \eta^{(n)}\right\}$–$\left\{\hat{\ell}_{1\text{–}6}^{(n)}\right\}$ in SM (2/1/0).

corr.	$\lvert V_{cb}\rvert$	$\xi^{(1)}$	$\xi^{(2)}$	$\hat{\chi}_2^{(0)}$	$\hat{\chi}_2^{(1)}$	$\hat{\chi}_3^{(1)}$	$\eta^{(0)}$	$\eta^{(1)}$
$\hat{\ell}_1^{(0)}$	−0.0096	−0.3082	0.3377	0.0696	−0.0916	−0.3307	0.2129	−0.1483
$\hat{\ell}_2^{(0)}$	−0.8276	−0.4799	0.2386	−0.0604	0.0459	0.5291	0.0913	0.0151
$\hat{\ell}_3^{(0)}$	0.0225	0.0183	−0.0229	−0.0291	−0.1991	−0.1191	−0.0119	−0.0307
$\hat{\ell}_4^{(0)}$	0.2246	0.0420	−0.0162	0.1489	0.0255	0.2770	−0.6829	−0.3803
$\hat{\ell}_5^{(0)}$	0.1837	0.3977	−0.2336	0.0896	0.1137	−0.1426	−0.3207	−0.0484
$\hat{\ell}_6^{(0)}$	0.0306	0.1684	−0.1027	0.0323	−0.0848	−0.1737	0.0029	0.0398

Table 11. Correlation among $\left\{\xi^{(n)},\, \hat{\chi}_{2,3}^{(n)},\, \eta^{(n)}\right\}$–$\left\{\hat{\ell}_{1\text{–}6}^{(n)}\right\}$ in SM (2/1/0).

corr.	$\hat{\ell}_1^{(0)}$	$\hat{\ell}_2^{(0)}$	$\hat{\ell}_3^{(0)}$	$\hat{\ell}_4^{(0)}$	$\hat{\ell}_5^{(0)}$	$\hat{\ell}_6^{(0)}$
$\hat{\ell}_1^{(0)}$	1.0000	0.0968	0.0519	0.1446	−0.1482	0.0144
$\hat{\ell}_2^{(0)}$	0.0968	1.0000	0.0288	−0.1439	−0.0969	0.0141
$\hat{\ell}_3^{(0)}$	0.0519	0.0288	1.0000	0.0166	0.1686	0.9515
$\hat{\ell}_4^{(0)}$	0.1446	−0.1439	0.0166	1.0000	0.2297	−0.0025
$\hat{\ell}_5^{(0)}$	−0.1482	−0.0969	0.1686	0.2297	1.0000	0.4106
$\hat{\ell}_6^{(0)}$	0.0144	0.0141	0.9515	−0.0025	0.4106	1.0000

Table 12. Correlation among $\left\{\hat{\ell}_{1\text{–}6}^{(n)}\right\}$–$\left\{\hat{\ell}_{1\text{–}6}^{(n)}\right\}$ in SM (2/1/0).

JHEP08(2020)006

References

[1] N. Cabibbo, *Unitary Symmetry and Leptonic Decays*, *Phys. Rev. Lett.* **10** (1963) 531 [INSPIRE].

[2] M. Kobayashi and T. Maskawa, *CP Violation in the Renormalizable Theory of Weak Interaction*, *Prog. Theor. Phys.* **49** (1973) 652 [INSPIRE].

[3] Belle-II collaboration, *The Belle II Physics Book*, *Prog. Theor. Exp. Phys.* **2019** (2019) 123C01 [*Erratum ibid.* **2020** (2020) 029201] [arXiv:1808.10567] [INSPIRE].

[4] I. Caprini, L. Lellouch and M. Neubert, *Dispersive bounds on the shape of $\bar{B} \to D^{(*)}\ell\bar{\nu}$ form-factors*, *Nucl. Phys. B* **530** (1998) 153 [hep-ph/9712417] [INSPIRE].

[5] N. Isgur and M.B. Wise, *Weak Decays of Heavy Mesons in the Static Quark Approximation*, *Phys. Lett. B* **232** (1989) 113 [INSPIRE].

[6] M. Neubert, *Heavy quark symmetry*, *Phys. Rept.* **245** (1994) 259 [hep-ph/9306320] [INSPIRE].

[7] C. Boyd, B. Grinstein and R.F. Lebed, *Precision corrections to dispersive bounds on form-factors*, *Phys. Rev. D* **56** (1997) 6895 [hep-ph/9705252] [INSPIRE].

[8] F.U. Bernlochner, Z. Ligeti, M. Papucci and D.J. Robinson, *Combined analysis of semileptonic B decays to D and D^*: $R(D^{(*)})$, $|V_{cb}|$ and new physics*, *Phys. Rev. D* **95** (2017) 115008 [*Erratum ibid.* **97** (2018) 059902] [arXiv:1703.05330] [INSPIRE].

[9] D. Bigi and P. Gambino, *Revisiting $B \to D\ell\nu$*, *Phys. Rev. D* **94** (2016) 094008 [arXiv:1606.08030] [INSPIRE].

[10] D. Bigi, P. Gambino and S. Schacht, *A fresh look at the determination of $|V_{cb}|$ from $B \to D^*\ell\nu$*, *Phys. Lett. B* **769** (2017) 441 [arXiv:1703.06124] [INSPIRE].

[11] B. Grinstein and A. Kobach, *Model-Independent Extraction of $|V_{cb}|$ from $\bar{B} \to D^*\ell\overline{\nu}$*, *Phys. Lett. B* **771** (2017) 359 [arXiv:1703.08170] [INSPIRE].

[12] S. Jaiswal, S. Nandi and S.K. Patra, *Extraction of $|V_{cb}|$ from $B \to D^{(*)}\ell\nu_\ell$ and the Standard Model predictions of $R(D^{(*)})$*, *JHEP* **12** (2017) 060 [arXiv:1707.09977] [INSPIRE].

[13] F.U. Bernlochner, Z. Ligeti, M. Papucci and D.J. Robinson, *Tensions and correlations in $|V_{cb}|$ determinations*, *Phys. Rev. D* **96** (2017) 091503 [arXiv:1708.07134] [INSPIRE].

[14] D. Bigi, P. Gambino and S. Schacht, *$R(D^*)$, $|V_{cb}|$ and the Heavy Quark Symmetry relations between form factors*, *JHEP* **11** (2017) 061 [arXiv:1707.09509] [INSPIRE].

[15] P. Gambino, M. Jung and S. Schacht, *The V_{cb} puzzle: An update*, *Phys. Lett. B* **795** (2019) 386 [arXiv:1905.08209] [INSPIRE].

[16] M. Jung and D.M. Straub, *Constraining new physics in $b \to c\ell\nu$ transitions*, *JHEP* **01** (2019) 009 [arXiv:1801.01112] [INSPIRE].

[17] M. Bordone, M. Jung and D. van Dyk, *Theory determination of $\bar{B} \to D^{(*)}\ell^-\bar{\nu}$ form factors at $\mathcal{O}(1/m_c^2)$*, *Eur. Phys. J. C* **80** (2020) 74 [arXiv:1908.09398] [INSPIRE].

JHEP08(2020)006

[18] Particle Data Group, *Review of Particle Physics*, *Phys. Rev. D* **98** (2018) 030001 [INSPIRE].

[19] Belle collaboration, *Measurement of the decay $B \to D\ell\nu_\ell$ in fully reconstructed events and determination of the Cabibbo-Kobayashi-Maskawa matrix element $|V_{cb}|$*, *Phys. Rev. D* **93** (2016) 032006 [arXiv:1510.03657] [INSPIRE].

[20] Belle collaboration, *Precise determination of the CKM matrix element $|V_{cb}|$ with $\bar{B}^0 \to D^{*+}\ell^-\bar{\nu}_\ell$ decays with hadronic tagging at Belle*, arXiv:1702.01521 [INSPIRE].

[21] Belle collaboration, *Measurement of the CKM matrix element $|V_{cb}|$ from $B^0 \to D^{*-}\ell^+\nu_\ell$ at Belle*, *Phys. Rev. D* **100** (2019) 052007 [arXiv:1809.03290] [INSPIRE].

[22] BaBar collaboration, *Extraction of form Factors from a Four-Dimensional Angular Analysis of $\overline{B} \to D^*\ell^-\overline{\nu}_\ell$*, *Phys. Rev. Lett.* **123** (2019) 091801 [arXiv:1903.10002] [INSPIRE].

[23] B. Carpenter, M.D. Hoffman, M. Brubaker, D. Lee, P. Li and M. Betancourt, *The Stan Math Library: Reverse-Mode Automatic Differentiation in C++*, arXiv:1509.07164.

[24] B. Carpenter et al., *Stan: A probabilistic programming language*, *J. Stat. Software* **76** (2017) 1 and online at https://mc-stan.org/.

[25] A. Gelman, J. Hwang and A. Vehtari, *Understanding predictive information criteria for Bayesian models*, arXiv:1307.5928.

[26] A.F. Falk and M. Neubert, *Second order power corrections in the heavy quark effective theory. 1. Formalism and meson form-factors*, *Phys. Rev. D* **47** (1993) 2965 [hep-ph/9209268] [INSPIRE].

[27] A. Sirlin, *Large m_W, m_Z Behavior of the $O(\alpha)$ Corrections to Semileptonic Processes Mediated by W*, *Nucl. Phys. B* **196** (1982) 83 [INSPIRE].

[28] Fermilab Lattice and MILC collaborations, *Update of $|V_{cb}|$ from the $\bar{B} \to D^*\ell\bar{\nu}$ form factor at zero recoil with three-flavor lattice QCD*, *Phys. Rev. D* **89** (2014) 114504 [arXiv:1403.0635] [INSPIRE].

[29] M. Tanaka and R. Watanabe, *New physics in the weak interaction of $\bar{B} \to D^{(*)}\tau\bar{\nu}$*, *Phys. Rev. D* **87** (2013) 034028 [arXiv:1212.1878] [INSPIRE].

[30] Y. Sakaki, M. Tanaka, A. Tayduganov and R. Watanabe, *Testing leptoquark models in $\bar{B} \to D^{(*)}\tau\bar{\nu}$*, *Phys. Rev. D* **88** (2013) 094012 [arXiv:1309.0301] [INSPIRE].

[31] Y. Sakaki, M. Tanaka, A. Tayduganov and R. Watanabe, *Probing New Physics with q^2 distributions in $\bar{B} \to D^{(*)}\tau\bar{\nu}$*, *Phys. Rev. D* **91** (2015) 114028 [arXiv:1412.3761] [INSPIRE].

[32] MILC collaboration, *$B \to D\ell\nu$ form factors at nonzero recoil and $|V_{cb}|$ from $2+1$-flavor lattice QCD*, *Phys. Rev. D* **92** (2015) 034506 [arXiv:1503.07237] [INSPIRE].

[33] HPQCD collaboration, *$B \to Dl\nu$ form factors at nonzero recoil and extraction of $|V_{cb}|$*, *Phys. Rev. D* **92** (2015) 054510 [*Erratum ibid.* **93** (2016) 119906] [arXiv:1505.03925] [INSPIRE].

[34] Flavour Lattice Averaging Group, *FLAG Review 2019: Flavour Lattice Averaging Group (FLAG)*, *Eur. Phys. J. C* **80** (2020) 113 [arXiv:1902.08191] [INSPIRE].

[35] N. Gubernari, A. Kokulu and D. van Dyk, *$B \to P$ and $B \to V$ Form Factors from B-Meson Light-Cone Sum Rules beyond Leading Twist*, *JHEP* **01** (2019) 150 [arXiv:1811.00983] [INSPIRE].

[36] M. Neubert, Z. Ligeti and Y. Nir, *QCD sum rule analysis of the subleading Isgur-Wise form-factor $\chi_2(v \cdot v')$*, *Phys. Lett. B* **301** (1993) 101 [hep-ph/9209271] [INSPIRE].

JHEP08(2020)006

[37] M. Neubert, Z. Ligeti and Y. Nir, *The Subleading Isgur-Wise form-factor $\chi_3(v \cdot v')$ to order α_s in QCD sum rules*, *Phys. Rev. D* **47** (1993) 5060 [hep-ph/9212266] [INSPIRE].

[38] Z. Ligeti, Y. Nir and M. Neubert, *The Subleading Isgur-Wise form-factor $\xi_3(v \cdot v')$ and its implications for the decays $\bar{B} \to D^{(*)}\ell\bar{\nu}$*, *Phys. Rev. D* **49** (1994) 1302 [hep-ph/9305304] [INSPIRE].

[39] E.J. Eichten and C. Quigg, *Mesons with Beauty and Charm: New Horizons in Spectroscopy*, *Phys. Rev. D* **99** (2019) 054025 [arXiv:1902.09735] [INSPIRE].

[40] Q. Li, M.-S. Liu, L.-S. Lu, Q.-F. Lü, L.-C. Gui and X.-H. Zhong, *Excited bottom-charmed mesons in a nonrelativistic quark model*, *Phys. Rev. D* **99** (2019) 096020 [arXiv:1903.11927] [INSPIRE].

[41] V. Picaud, *MathematicaStan*, (2020) https://mc-stan.org/users/interfaces/mathematica-stan.

[42] HFLAV collaboration, *Averages of b-hadron, c-hadron and τ-lepton properties as of 2018*, arXiv:1909.12524 [INSPIRE].

[43] Belle collaboration, *Measurement of the D^{*-} polarization in the decay $B^0 \to D^{*-}\tau^+\nu_\tau$*, in proceedings of the *10th International Workshop on the CKM Unitarity Triangle (CKM 2018)*, Heidelberg, Germany, 17–21 September 2018, [arXiv:1903.03102] [INSPIRE].

[44] A. Crivellin, *Effects of right-handed charged currents on the determinations of $|V_{ub}|$ and $|V_{cb}|$*, *Phys. Rev. D* **81** (2010) 031301 [arXiv:0907.2461] [INSPIRE].

[45] A. Crivellin and S. Pokorski, *Can the differences in the determinations of V_{ub} and V_{cb} be explained by New Physics?*, *Phys. Rev. Lett.* **114** (2015) 011802 [arXiv:1407.1320] [INSPIRE].

[46] A. Greljo, J. Martin Camalich and J.D. Ruiz-Álvarez, *Mono-τ Signatures at the LHC Constrain Explanations of B-decay Anomalies*, *Phys. Rev. Lett.* **122** (2019) 131803 [arXiv:1811.07920] [INSPIRE].

[47] ATLAS collaboration, *Search for High-Mass Resonances Decaying to $\tau\nu$ in pp Collisions at $\sqrt{s} = 13$ TeV with the ATLAS Detector*, *Phys. Rev. Lett.* **120** (2018) 161802 [arXiv:1801.06992] [INSPIRE].

[48] CMS collaboration, *Search for a W' boson decaying to a τ lepton and a neutrino in proton-proton collisions at $\sqrt{s} = 13$ TeV*, *Phys. Lett. B* **792** (2019) 107 [arXiv:1807.11421] [INSPIRE].

[49] W. Altmannshofer, P.S. Bhupal Dev and A. Soni, *$R_{D^{(*)}}$ anomaly: A possible hint for natural supersymmetry with R-parity violation*, *Phys. Rev. D* **96** (2017) 095010 [arXiv:1704.06659] [INSPIRE].

[50] S. Iguro and K. Tobe, *$R(D^{(*)})$ in a general two Higgs doublet model*, *Nucl. Phys. B* **925** (2017) 560 [arXiv:1708.06176] [INSPIRE].

[51] M. Abdullah, J. Calle, B. Dutta, A. Flórez and D. Restrepo, *Probing a simplified, W' model of $R(D^{(*)})$ anomalies using b-tags, τ leptons and missing energy*, *Phys. Rev. D* **98** (2018) 055016 [arXiv:1805.01869] [INSPIRE].

[52] S. Iguro, Y. Omura and M. Takeuchi, *Test of the $R(D^{(*)})$ anomaly at the LHC*, *Phys. Rev. D* **99** (2019) 075013 [arXiv:1810.05843] [INSPIRE].

[53] M.J. Baker, J. Fuentes-Martín, G. Isidori and M. König, *High-p_T signatures in vector-leptoquark models*, *Eur. Phys. J. C* **79** (2019) 334 [arXiv:1901.10480] [INSPIRE].

JHEP08(2020)006

[54] ATLAS collaboration, *Search for a heavy charged boson in events with a charged lepton and missing transverse momentum from pp collisions at $\sqrt{s} = 13$ TeV with the ATLAS detector*, *Phys. Rev. D* **100** (2019) 052013 [arXiv:1906.05609] [INSPIRE].

[55] S. Iguro, T. Kitahara, Y. Omura, R. Watanabe and K. Yamamoto, *D^* polarization vs. $R_{D^{(*)}}$ anomalies in the leptoquark models*, *JHEP* **02** (2019) 194 [arXiv:1811.08899] [INSPIRE].

[56] M. Blanke et al., *Impact of polarization observables and $B_c \to \tau\nu$ on new physics explanations of the $b \to c\tau\nu$ anomaly*, *Phys. Rev. D* **99** (2019) 075006 [arXiv:1811.09603] [INSPIRE].

[57] BELLE collaboration, *Measurement of the τ lepton polarization and $R(D^*)$ in the decay $\bar{B} \to D^*\tau^-\bar{\nu}_\tau$*, *Phys. Rev. Lett.* **118** (2017) 211801 [arXiv:1612.00529] [INSPIRE].

[58] C. Murgui, A. Peñuelas, M. Jung and A. Pich, *Global fit to $b \to c\tau\nu$ transitions*, *JHEP* **09** (2019) 103 [arXiv:1904.09311] [INSPIRE].

[59] S. Jaiswal, S. Nandi and S.K. Patra, *Updates on extraction of $|V_{cb}|$ and SM prediction of $R(D^*)$ in $B \to D^*\ell\nu_\ell$ decays*, *JHEP* **06** (2020) 165 [arXiv:2002.05726] [INSPIRE].

[60] K. Cheung, Z.-R. Huang, H.-D. Li, C.-D. Lü, Y.-N. Mao and R.-Y. Tang, *Revisit to the $b \to c\tau\nu$ transition: in and beyond the SM*, arXiv:2002.07272 [INSPIRE].

[61] J. De Blas et al., *HEPfit: a code for the combination of indirect and direct constraints on high energy physics models*, *Eur. Phys. J. C* **80** (2020) 456 [arXiv:1910.14012] [INSPIRE].

[62] B. Bhattacharya, A. Datta, S. Kamali and D. London, *CP Violation in $\bar{B}^0 \to D^{*+}\mu^-\bar{\nu}_\mu$*, *JHEP* **05** (2019) 191 [arXiv:1903.02567] [INSPIRE].

[63] S. de Boer, T. Kitahara and I. Nisandzic, *Soft-Photon Corrections to $\bar{B} \to D\tau^-\bar{\nu}_\tau$ Relative to $\bar{B} \to D\mu^-\bar{\nu}_\mu$*, *Phys. Rev. Lett.* **120** (2018) 261804 [arXiv:1803.05881] [INSPIRE].

[64] P. Colangelo and A. Khodjamirian, *QCD sum rules, a modern perspective*, in *At the frontier of particle physics. Volume 3*, M. Shifman ed., World Scientific (2001), pp. 1495–1576 [hep-ph/0010175] [INSPIRE].

[65] B.L. Ioffe, *QCD at low energies*, *Prog. Part. Nucl. Phys.* **56** (2006) 232 [hep-ph/0502148] [INSPIRE].

[66] Z.-G. Wang, *Analysis of the decay constants of the heavy pseudoscalar mesons with QCD sum rules*, *JHEP* **10** (2013) 208 [arXiv:1301.1399] [INSPIRE].

[67] S. Narison, *QCD parameter correlations from heavy quarkonia*, *Int. J. Mod. Phys. A* **33** (2018) 1850045 [*Addendum ibid.* **33** (2018) 1892004] [arXiv:1801.00592] [INSPIRE].

[68] V.M. Belyaev and B.L. Ioffe, *Determination of Baryon and Baryonic Resonance Masses from QCD Sum Rules. 1. Nonstrange Baryons*, *Sov. Phys. JETP* **56** (1982) 493 [*Zh. Eksp. Teor. Fiz.* **83** (1982) 876] [INSPIRE].

[69] H.G. Dosch and S. Narison, *Direct extraction of the chiral quark condensate and bounds on the light quark masses*, *Phys. Lett. B* **417** (1998) 173 [hep-ph/9709215] [INSPIRE].

[70] A. Di Giacomo and Y. Simonov, *The Quark gluon mixed condensate calculated via field correlators*, *Phys. Lett. B* **595** (2004) 368 [hep-ph/0404044] [INSPIRE].

JHEP08(2020)006